# SPATIAL RELATION BETWEEN MAIN EARTHQUAKE SLIP AND ITS AFTERSHOCK DISTRIBUTION

S. Das and C. Henry[1]
*Department of Earth Sciences, University of Oxford, Oxford, UK*

Received 16 October 2002; revised 12 May 2003; accepted 26 June 2003; published 27 September 2003.

[1] We examine where aftershocks occur relative to the spatial distribution of the main shock slip using data from several recent large earthquakes. No universal relation between high- and low-moment regions and high or low aftershock occurrence, or vice versa, is found. We generally find that few, and usually the smaller, aftershocks occur in the high-slip regions of the fault, a notable exception to this being the great 1996 Biak, Indonesia, subduction zone earthquake. In all cases, aftershocks occur on favorably oriented planes of weakness in regions of increased postseismic stress. Generally, they are clustered at both ends of faults, but examples where aftershocks occur only at one end or where there is no clustering at the ends are found. Aftershock clusters are also found at the edge of unbroken barriers, and regions of rapid transition from high to low slip, within the main fault area. We identify examples of geometrical and inhomogeneous barriers and sharp and dull stress concentrations. Rupture in the main shock is generally found to nucleate in the region of low slip or at the edge of high-slip regions, the 1996 Biak earthquake again being the only exception, nucleating in a very high slip region. Off-fault aftershocks are found for all earthquakes in this study, and they sometimes rupture the nodal plane conjugate to the main shock fault plane.
*INDEX TERMS:* 7209 Seismology: Earthquake dynamics and mechanics; 7215 Seismology: Earthquake parameters; 7230 Seismology: Seismicity and seismotectonics; *KEYWORDS:* aftershocks, earthquake slip, stress changes, barriers
**Citation:** Das, S., and C. Henry, Spatial relation between main earthquake slip and its aftershock distribution, *Rev. Geophys., 41*(3), 1013, doi:10.1029/2002RG000119, 2003.

## 1. INTRODUCTION

[2] It has now been known for more than a century that aftershocks occur on and around the main shock region. The first formal study of aftershocks was made by *Omori* [1894] for the 1891 Mino-Owari (Nobi), Japan, earthquake. He found that more than 3000 aftershocks were recorded in the 26-month period following the earthquake, and his observations led him to postulate the law, now called the Omori law, showing that the frequency of aftershocks dies off hyperbolically after the main earthquake (see *Milne and Lee* [1939] and *Scholz* [1989] for more recent discussions). That is, if $N$ is the number of aftershocks and $t$ is the time measured from the main shock, then

$$N = \frac{c_1}{t + c_2},$$

where $c_1$ and $c_2$ are constants.

[3] Though the cumulative seismic moment for aftershocks is usually negligible (usually only a few percent) compared to the main shock, aftershocks have been disproportionately heavily studied, because once one knows where a large earthquake has occurred, arrays of seismometers can be installed rapidly in the epicentral region to "catch" the aftershocks, and "aftershock chasing" is now a seismic sport! This is very fortunate as aftershocks provide valuable information about the main shock, among the most important being a good estimate of the main shock fault area. *Richter* [1955] was the first to directly link the rupture area of the earthquake to the aftershock distribution based on his study of the aftershocks of the $M_s$ 7.6–7.7 21 July 1952 Kern County (Arvin-Tehachapi), California, earthquake, for which portable seismometers were deployed in the epicentral region within hours of the main shock. The earthquake occurred on a fault dipping ~60°. To quote from *Richter* [1955], "… the epicenters … are distributed over a roughly rectangular area …. This suggests a rectangular outline in plan for the crustal block displaced in the main event …." Since then, aftershock areas have been widely used as estimates of the main shock fault area. In fact, even as recently as 1989 and for as large an earthquake as the $M_w$ 8.0 Macquarie Ridge earthquake, the best estimate of the rupture area was from the aftershocks, as the low number and the then still poor azimuthal distribution of high-quality broadband digital stations were

[1]Now at Oxford Computer Consultants, Oxford, U.K.




8755-1209/03/2003RG000119*$15.00* doi:10.1029/2002RG000119

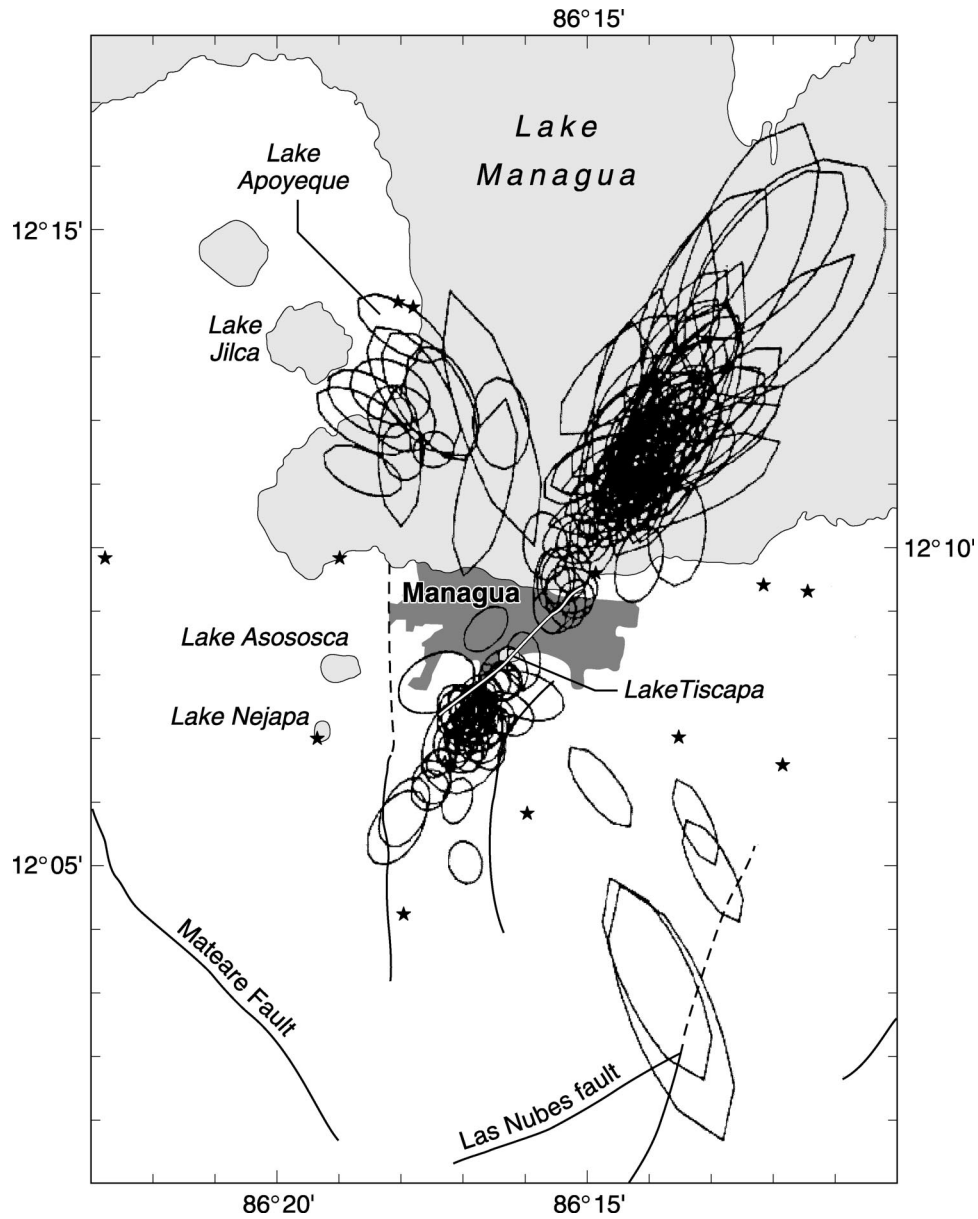


**Figure 1.** Aftershock distribution of the 23 December 1972 $M_w$ 6.3 left-lateral strike-slip Managua, Nicaragua, earthquake (taken from *Ward et al.* [1974], ©Seismological Society of America). The 171 reliably located aftershocks (with at least six *P* wave arrival times) are shown for the period 3 January 1973 to 7 February 1973. The moment magnitude for the main shock is taken from the new catalog of *Perez* [1999] (available at http://www.ldc.usb.ve/~ojperez/catalog). The polygons represent the 68% confidence limits in location. Station locations are shown by stars. The white line outlined in black is the main shock fault. The solid lines represent other faults mapped at the surface.

not sufficient to constrain the rupture area from the waves recorded on the seismograms [*Das*, 1993]. It is only since the mid-1990s that the wide deployment of broadband stations worldwide, particularly in remote locations, finally has allowed the rupture area to be directly obtained unambiguously by a formal seismogram inversion [*Henry et al.*, 2000; *Henry*, 2002].

[4] Until very good quality seismograms and reliable Earth structure became available, the aftershock distributions looked like clouds around the main shock rupture area. With improvement in determining earthquake locations in the last 20 or so years, due both to better quality and more numerous seismograms as well as better knowledge of Earth structure, we have come to see much clearer patterns in the aftershock distributions. (Comparing Figures 4–9 and 4–10 of *Yeats et al.* [1997] for the seismicity of southern California for the years 1932 and 1990, respectively, is very instructive in this respect.) From the patterns that have now emerged, we can identify three distinct regions where aftershocks occur. First, they occur at the ends of faults; usually, these are the densest clusters, and usually, though not

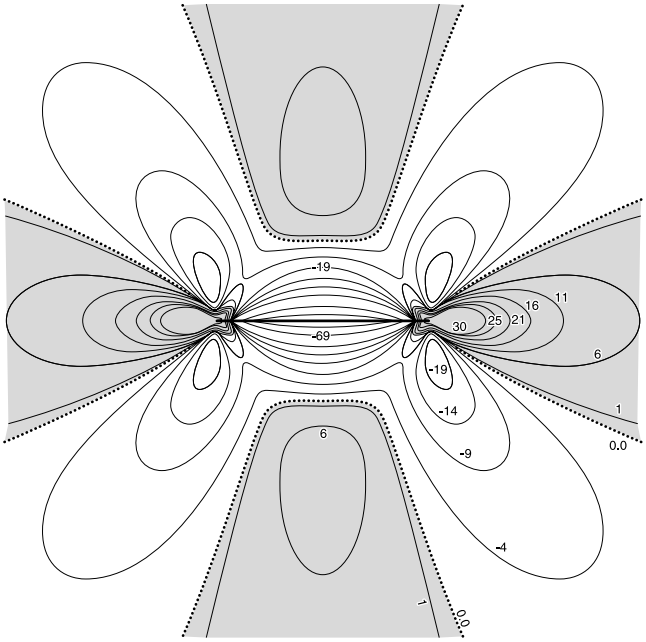


**Figure 2.** Shear stress change due to an in-plane shear fault in an infinite, homogeneous, elastic medium (taken from *Kostrov and Das* [1982]). The shaded areas are regions of stress increase, and the unshaded areas are regions of stress decrease. The contour lines are labeled with the stress change as a percentage of the stress drop on the fault (shown by the bold solid line); the line of no stress change is shown by the dotted lines. Note that in theory one should really plot the quantity (shear stress plus μ times normal stress), the Coulomb failure criterion, μ being the coefficient of friction, as is often done. Such a figure would depend on the values of μ and the normal stress. Note also that such figures would be asymmetric on the two sides of the fault. The remarkable similarity between Figures 2 and 1, which shows a very slight asymmetry of the aftershocks (those on the northern side are shifted slightly to the right), may actually imply that the second term in the Coulomb criterion is less significant.

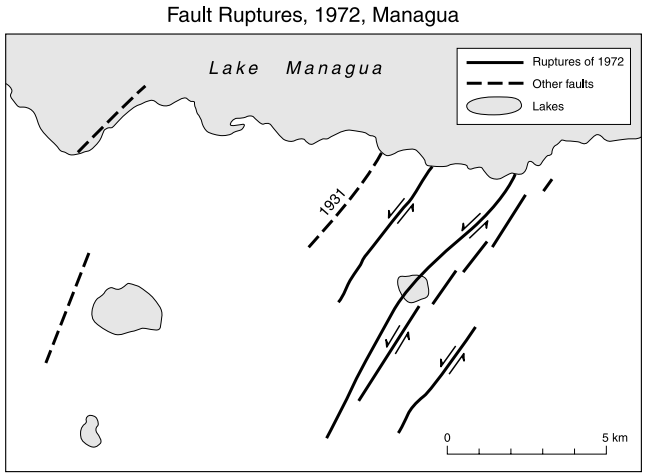


**Figure 3.** The main left-lateral strike-slip fault and several similar faults parallel to it in the epicentral region of the 1972 Managua, Nicaragua, earthquake, whose aftershocks are shown in Figure 1 (modified from Figure 8–33 of *Yeats et al.* [1997], used by permission of Oxford University Press, Inc.)

always, they have the largest aftershocks. Next, they occur over the entire fault area. Finally, aftershocks occur off the main fault in a direction perpendicular to it; these are often the fewest and smallest in magnitude, though examples of earthquakes with large off-fault aftershocks are known. The 1972 Managua, Nicaragua, earthquake ($M_w$ = 6.3) is a classic example showing all three types of aftershocks (Figure 1). Clustering of aftershocks at the ends of the fault was also clearly seen for the 1952 Kern County earthquake [*Benioff*, 1955].

[5] On the basis of our understanding of the mechanics of earthquakes and on models of faulting we now know that aftershocks occur in regions where the stress has increased because of the occurrence of the main shock. The shear stress change due to an in-plane fault with a uniform stress drop is shown in Figure 2 [from *Kostrov and Das*, 1982]. The primary and largest stress increase is generally at the ends of the main shock rupture. The next level of stress increase, obtained from dynamic models of faulting with variable stress drop on the fault, shows many complexities in the stress distribution on the main rupture area [*Mikumo and Miyatake*, 1979; *Madariaga*, 1979; *Das and Kostrov*, 1988; *Cochard and Madariaga*, 1994, 1996] and increased stress on unbroken or less slipped regions of the rupture area. Similar stress increases are expected in regions of transition from higher to lower slip on the main fault, that is, regions with large slip gradients. In fact, it is the observation that aftershocks do occur over the main fault rupture area that provides direct proof that earthquake faults are indeed heterogeneous and have very nonuniform slip across the fault plane. Last, there is a small stress increase in some off-fault locations. Except at the edges of the fault the stress increase due to the main shock is generally small and cannot usually cause earthquakes by rupture of virgin rock. Thus, except at these places, aftershocks can only occur on favorably oriented preexisting planes of weakness, and increased stresses in markedly different directions will not lead to aftershocks. Of course, even at the edges of the fault, aftershocks will occur on the most optimally oriented preexisting weak planes. That the existence of these preexisting weak planes is more important than the stress direction is well known to geologists; *Yeats et al.* [1997, p. 27] state that "it is rare to find a … rock mass … in which a fault was initiated whose orientation is controlled solely by the orientation of the principal stresses and the coefficient of static friction" and that a recurrence of displacement is likely along preexisting planes of weakness "even if the stress field changes to some degree." Obviously, the most favorably oriented planes are close to parallel to either the main shock rupture plane or to its conjugate. The principal favorably oriented plane is, of course, the main shock fault plane itself, both for continuations of the causative fault beyond the rupture terminations as well as for regions with

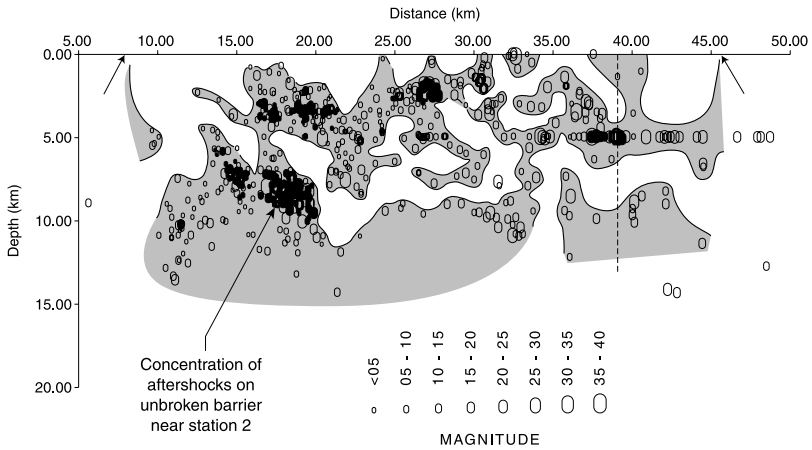


**Figure 4.** Hypocenters of the magnitude 6.4 28 June 1966 Parkfield, California, earthquake projected onto the vertical fault plane, based on the data of *Eaton et al.* [1970]. The hypothetical boundary between slipped regions (regions with no aftershocks, shown unshaded) and the unbroken areas (region with aftershocks, shown shaded) was drawn by *Aki* [1979]. The ends of the zones of surface fracture are shown by arrows. The vertical dotted line indicates the approximate position of the main shock epicenter. Note the concentration of aftershocks on the unbroken barrier near station 2.

high-slip gradients on the rupture area. Planes of weakness parallel and perpendicular to the main shock rupture plane in the off-fault regions of increased stress arise naturally in various tectonic settings. The multiple strands of the San Andreas fault system provide closely spaced parallel planes of weakness. Figure 3 shows the parallel faults of 1972 Managua earthquake. Many conjugate fault systems exist in Japan (see Figure 8–10 of *Yeats et al.* [1997] for some examples). The $M_w$ 7.1 1927 Tango, Japan, earthquake ruptured on two conjugate faults [*Richter*, 1958]. Earthquakes on oceanic transform faults or fossil fracture zones have a preexisting ridge fabric emplaced at the time of formation of the oceanic crust, which is nearly perpendicular to the main fault plane. Thus whether or not an aftershock occurs at a given place depends both on whether there are preexisting weak planes there, as well as on the existence of favorably oriented stress increase on such planes.

[6] It is generally believed that aftershock areas are not static but expand with time. *Tajima and Kanamori* [1985] used aftershocks located through the National Earthquake Information Center (NEIC) for 44 large earthquakes from 1963 to 1980, and by contouring the energy released by the aftershocks, they concluded that some aftershock areas do expand with time, whereas others do not. *Pegler and Das* [1996a] and *Henry and Das* [2001] have relocated the aftershocks of 94 large earthquakes in the period 1977–2000, using the joint hypocenter determination (JHD) method and tabulated the aftershock zone length for different periods following the main shock, such as, the 1-day, 7-day, and 30-day periods. Examination of the detailed maps of *Pegler* [1995] and *Henry* [2002] shows that there is generally little change in the aftershock area after the first week, the later aftershocks simply filling in the area established early. Figures 2 and 3 of *Henry and Das* [2001] illustrate this by a comparison of the aftershock lengths for the 1-day and 30-day periods for the 94 earthquakes. We shall compare the fault area obtained from inverting the waveforms with the aftershock zones for different periods later in the paper for two large earthquakes, namely, the 1998 Antarctic earthquake and the 1996 Biak earthquake.

[7] In relatively simple tectonic settings with strike-slip faulting the aftershocks that are large enough to have known focal mechanisms, in general, have mechanisms similar to that of the main shock. In more complex tectonic areas, such as subduction zones, a thrust main shock can have aftershocks with thrust, normal, or strike-slip mechanisms. Aftershocks at the end of faults seldom have fault plane solutions significantly different from that of the main shock. *Mendoza and Hartzell* [1988a] made use of this criterion to decide if the aftershocks at the fault edges were extending the main fault or were due to more complex perturbations of the local stress field in their study of several moderate to large earthquakes from the United States.

[8] On the basis of the "barrier model" of heterogeneous earthquake faulting [*Das and Aki*, 1977], *Aki* [1979] wrote "… we expect few aftershocks over a section of fault slipped smoothly and many aftershocks over a section with little slip where increased stress concentration causes a sequence of aftershocks by static fatigue …." In this now classic paper, Aki identified the regions of the fault for the 1966 Parkfield, California, earthquake that slipped smoothly and the unbroken barrier near the southern end over which the earthquake jumped and which had the highest concentration of aftershocks by contouring regions of high and low aftershock occurrence within the fault area of the earthquake (Figure 4). Until relatively recently, it was not possible to even check if aftershocks really do concentrate on re-

gions of low slip by comparing the aftershock locations with the fault slip. This was due to both the errors in earthquake locations and the lack of data to determine the details of fault slip. However, in the last decade or so, owing to the availability of seismic data of sufficiently high quality and sufficient spatial coverage to resolve many details of earthquake ruptures, several studies have estimated the actual slip distribution on the rupture plane of large earthquakes. Studies by *Mendoza and Hartzell* [1988a, 1988b, 1989] were early attempts at this. Using the slip distributions for several moderate to large earthquakes together with their aftershock distributions, they concluded that the aftershocks occurred mostly outside or near the edges of the areas of large slip. Note that in discussions in this paper we shall use the terms "slip distribution" and "moment distribution" on the fault interchangeably, the two being related simply by the modulus of rigidity of the medium. On the basis of a few such examples it is now widely believed that "… that part of the fault characterized by the slip during the earthquake[s] has relatively few aftershocks" [*Yeats et al.*, 1997, p. 45].

[9] *Aki* [1979] classified barriers as "geometric" and "inhomogeneous," the former being places where the fault changes direction and the latter being places where no obvious geometrical discontinuity can be identified, so that the barrier is due to change in the strength properties of the rocks. He also identified barriers as being "sharp" and "dull" stress concentrators, with the sharpest stress concentrator being a barrier between twin earthquakes. On the basis of fracture mechanical considerations we can also consider sharp stress concentrators as those (strong) barriers where earthquakes abruptly stop, the stress distribution in that case having the classical sharp falloff at the fault edge ($1/\sqrt{r}$ shape very close to the edge, $r$ being the distance beyond the fault edge). On the other hand, we know that earthquakes can also stop by propagating into regions where there is no stress [*Husseini et al.*, 1975; *Das*, 1976] (see the paper by *Dmowska and Rice* [1985] for a review of the latter results). For example, along plate boundaries a great earthquake may stop by running into the adjacent regions that were broken in recent earthquakes, that is, by running out of strain energy. In this case, one does not get the sharp falloff in stress with distance from the fault edge but a gentler one, leading to a lower and more distributed stress concentration compared to the former case where the stress concentration is larger and more localized. We shall use the shape of the falloff of slip with distance as one approaches the edges of the fault from its interior (this, of course, is directly related to the shape of the falloff of stress with distance outside the fault edge), when sufficiently well resolved, as the criterion to decide if we expect a sharp or dull stress concentration at the fault ends. Whether or not aftershocks cluster at the end of faults may depend on the sharpness of the rupture termination; obviously, the sharper ones are expected to have more aftershocks than the duller concentrators. So we shall use this as the test of our identification of the sharpness or dullness of the barrier, when possible.

[10] The availability of reliable data makes this a good time to stop and review the results. In this paper, we examine the relation between the regions of high and low slip on faults and the locations of aftershocks using the solutions from several earthquakes that have occurred since the work of *Mendoza and Hartzell* [1988a, 1988b, 1989]. This will allow us to determine if any simple correlation exists between aftershock location and high- and low-slip regions on the main shock fault, to test directly if some of the implications of the barrier model generally hold, and to see if the main conclusions of *Mendoza and Hartzell* [1988a, 1988b, 1989] hold for these recent earthquakes. For many of the earthquakes in this study we shall distinguish between geometric and inhomogeneous barriers and examine both the slip and aftershock distributions to see if we can recognize sharp and dull stress concentrators.

[11] There is a very practical reason why it is necessary to understand the relation between regions of high and low slip and regions of aftershocks. For very great earthquakes that occurred before 1964, aftershock information is available but not the moment distribution, and the former has been used to infer the latter. An example is the study by *Boyd et al.* [1995], in which the two great earthquakes in 1957 and 1986 along the Aleutians subduction zone (discussed in section 2.6) are compared in order to understand the moment release along that plate boundary over a complete seismic cycle. The moment distribution of the 1957 earthquake is guessed by assuming that "moment release is located in regions producing few aftershocks." That one has to be careful when doing this will be shown from a recent example of a great subduction zone earthquake where this is clearly not true.

[12] Before proceeding further, it is instructive to discuss currently available resolution in determining the slip distribution for large earthquakes. To quote from *Lay and Wallace* [1995, p. 310],

> Knowledge of the propagation effects [of seismic waves in the Earth] allows us to constrain the physical properties of the source. This is a startling proposition: to use the limited sampling of seismic wave-fields provided by seismometers located sparsely on the surface to deduce complex transient phenomena that have taken place thousands of kilometers away perhaps at great depth, in a medium as complicated as the Earth!

[13] It is important to keep this in mind when discussing the current limits of resolution of the slip on a fault, and seismologists' goal of obtaining an increasingly higher level of detail is not to be interpreted as them having forgotten what has been achieved. It is only the fact that some questions will still remains unanswered that is being mentioned here and the causes of the limitations on resolution that is being discussed. We note here only that some questions will remain unanswered, and we discuss the causes of the limitations on

resolution. To determine the details of the slip distribution history due to an earthquake, one solves the "inverse problem" of determining this from analyzing body wave seismograms. Usually, one uses the *P* and the *SH* waves in the period range ~2–120 s. The fault area is divided into cells, and the time at the source is divided into time steps. Replacing the integrals by summations in the integral equation relating seismograms to the fault slip rate, one obtains the system of linear equations $A\mathbf{x} \approx \mathbf{b}$, where $\mathbf{x}$ is the vector of unknown fault slip rates at each grid and at each time step, $\mathbf{b}$ is the vector of the digitally recorded seismograms, and the matrix $A$ is the impulse response of the Earth medium (the Green functions) and depends on the Earth structure. Additional conditions such as causality, not allowing the fault to slip backward, etc., can be used to improve the stability of the solution. The seismic moment of the centroid moment tensor (CMT) solution, obtained from much longer period waves, has also been used as a constraint in the late 1980s, but nowadays the data have become so much better that it is not necessary to preassign it, and the seismic moment can be obtained as part of the solution. More technical details of this can be found in the work of *Olson and Apsel* [1982], *Hartzell and Heaton* [1983], *Das and Kostrov* [1990, 1994], and *Das et al.* [1996]. The solution is obtained by minimizing the difference between the left and right sides of the system of equations, that is, between the data and the model. In the past, mainly because of insufficient computer size, some parameters, such as rupture velocity, were often preassigned to reduce the size of the matrix $A$. This had the effect of obtaining one solution, fitting the data, and excluding other equally physically plausible solutions, also fitting the data. Nowadays, no such preassignments are made, and the details, such as the fault area, slip distribution, rupture velocity, etc., are being found as part of the solution.

[14] When interpreting the results, the instability of the solution must be kept in mind. *Das and Kostrov* [1990, 1994] discussed this fully in their study of the 1989 Macquarie Ridge earthquake. They suggested that the parameterization of the problem should be very flexible, the solution should fit the data well, and constraints should then be added in stages to obtain solutions with some desirable feature, such as a smooth solution. Many solutions fitting the data equally well for practical purposes can be obtained in this way and inspected, and only robust features common to all solutions should be interpreted. *Das and Kostrov* [1994] also suggested that if a particular feature is crucial to an interpretation, a formal attempt should be made to find well-fitting solutions that do not contain the feature, and they developed methods to do this. Only if such a test is made and shows that no such solutions exist, may it then be said that the feature is required to explain the data. This is the procedure followed in recent studies of great earthquakes, such as the 1998 Antarctic plate earthquake [*Henry et al.*, 2000] and the 1996 Biak earthquake [*Henry and Das*, 2002], where many tens of solutions have been obtained and examined and, for example, precise limits placed on the extent of rupture that is required to explain the data.

[15] With the current resolution we are now able to determine the main features of the slip distribution even on faults located deep within the oceanic plates and far from seismometers. The smaller-scale variations are currently often detectable but not yet completely resolvable by the frequency of waves used in the studies. These frequencies, among other things, are also those for which the Earth structure is believed to be reliably known. The grid sizes used in the studies vary from 20 km in space and 5 s in time for the earlier earthquakes used in this paper (e.g., the 1989 Macquarie Ridge earthquake) to 10 km and 3-s grids for the very recent earthquakes (e.g., the 1998 Antarctic earthquake), showing that the resolution is improving with time. For the latter earthquake, extensive tests were carried out by inspecting the Green functions at adjacent cells to see how similar the Green functions were. Too similar Green functions (i.e., too small cells) lead to almost identical columns in the matrix $A$ being inverted, causing obvious problems of ill conditioning [*Das et al.*, 1996]. The spatial and temporal grid sizes should also be consistent with the wave speeds of the waves being inverted. One of the problems with the current resolution is that it is sometimes not possible to say if a small amount of slip is occurring, either within the main fault area or beyond the identified fault terminations. The former limits our ability to say whether some part within the fault is completely locked with no slip on it at all or whether it has some small amount of slip. The latter may appear to be a problem when considering how the ruptures terminate at both ends and whence sharp and dull stress concentrators could be identified. We shall not consider very small slip beyond the fault ends to be real in the interpretations in this paper. In some of the more detailed studies carried out by us earlier [*Henry et al.*, 2000; *Henry*, 2002], we have actually shown that we can fit the seismograms equally well without this small slip. The even higher resolution of the slip distribution on the fault that is desirable for such purposes is limited by the still relatively sparse global seismic station distribution, though a few places in the world such as California and Japan are heavily instrumented. A less important factor is the size and speed of today's supercomputers, though this is increasing continually. In spite of these limitations, with the currently available resolution one can at least begin to answer some of the detailed questions which have existed for decades.

[16] It may also be useful to mention briefly here the improvements that have occurred in finding the positions of the aftershocks. The locations obtained by agencies, such as the NEIC and the International Seismological Centre, as well as those obtained by *Engdahl et al.* [1998], are absolute locations and are therefore still dependent on knowledge of Earth structure. On the other hand, using a method of finding the locations of

the aftershocks relative to the epicenter of the main shock minimizes the effect of Earth structure, which is still unknown at high frequencies and particularly for submarine areas where most earthquakes occur after all. Such a method is the JHD method [*Douglas*, 1967; *Dewey* 1971, 1983] in which the seismic body wave phase arrival times reported by agencies are used and one has to solve another "inverse problem" involving inversion of a large matrix. For the earthquakes discussed in detail in this review, the JHD locations are used.

[17] We consider in-depth seven large recent earthquakes, chosen because in each case their slip distribution and history has been obtained by a formal inversion of the seismograms, carried out either by us in previous studies or by other authors. Since most of the earthquakes are studied teleseismically, we only consider aftershocks of magnitude >5, as it is not possible to relocate reliably smaller aftershocks of distant earthquakes. In one case (the 1992 Landers, California, earthquake) we have used aftershock distributions from local studies, and in that case all available aftershocks are shown, but only the ones of magnitude >5 are used in the interpretation. In any case, small aftershocks represent fine and very complex irregularities of the fault surface and stress distribution, and since we are currently still at the stage of obtaining the broad picture, we do not look at such short wavelength phenomena.

## 2. AFTERSHOCKS ON AND NEAR THE MAIN FAULT PLANE

[18] This is the location where generally the most and largest aftershocks occur. These aftershocks usually occur within a zone of a few to at most a very few tens of kilometers width around the main shock rupture plane. So we discuss individually the details of their distributions for the seven earthquakes of this study, first, the strike-slip earthquakes in chronological order and then the dip-slip ones. The CMT solutions, which give the faulting mechanism, are shown for each earthquake. Some of these are taken from *Dziewonski et al.* [1983–1999], while others were determined independently. It should be remembered that these solutions fit the amplitude and waveform of the entire long-period (frequency <1/135 Hz) seismogram [*Dziewonski and Woodhouse*, 1983] and are not the *P* wave first-motion solutions available for earthquakes before the mid-1970s, and hence they are much more reliable.

### 2.1. $M_w$ 8.0 1989 Strike-Slip Macquarie Ridge Earthquake (Figure 5)

[19] At the time of its occurrence the $M_w$ 8.0 1989 strike-slip Macquarie Ridge earthquake was the largest global seismic event to have occurred for ~12 years and the largest on the India/Australia-Pacific plate boundary south of New Zealand in >70 years. The tectonic interpretation of the earthquake mechanisms combined with the locations of all known earthquakes in the area was used by *Das* [1993] to suggest that the triangular area between the plate boundary, a reactivated fracture to the west of the plate boundary and a fault to the north on which an earthquake of magnitude ($M_s$ = 7.7) occurred in 1982, is being "squeezed" toward the north and west (Figures 5a and 5b). This triangular feature is clearly seen in gravity anomaly maps of the region.

[20] This earthquake was the first for which the method of formal investigation of the instability of the solution was developed and applied [*Das and Kostrov*, 1990, 1994]. Das and Kostrov first demonstrated the instability and then showed how physically based constraints can be added to stabilize the problem. They also showed how robust features of the solution persist over many solutions with different sets of constraints, and they only considered these features in their tectonic interpretation. The rupture was found to have propagated bilaterally for ~200 km, its average speed being the shear wave speed of the medium. The earthquake was characterized by its relative lack of aftershocks [*Das*, 1993] compared to, say, the 1986 Andreanof Islands earthquake, both being of comparable magnitude and occurring only 3 years apart (this latter fact implying that the detection threshold was the same for both earthquakes). No aftershock clusters are seen at the ends of the main rupture, though an aftershock with the same focal mechanism as the main shock on the main fault plane occurred at the northern end (the northernmost CMT solution on the plate boundary in Figure 5a). The number of aftershocks on the main fault plane was greatest just north of its intersection with a preexisting fault [*Das*, 1993; *Das and Kostrov*, 1994], which was also a region of low slip in the main shock. This preexisting fault was reactivated by the main shock, and the reason for this clustering can be interpreted as being due to the increased stress in the triangular region bounded by the two intersecting (the main plate boundary and the reactivated) faults. *Das* [1992] identified the southern termination of the earthquake rupture as being due to a geometrical barrier where there was major change in the plate boundary direction. The northern end could be an inhomogeneous barrier. On the basis of the gentler falloff of slip at the northern end and the very high slip at the southern end the former is a dull stress concentrator, and the latter is a sharp stress concentrator. However, there is a small aftershock at the northern end (identified above) and none at the southern end (Figure 5a), which is the reverse of what one would expect for the sharp and dull stress concentrators, showing that either the relation between these is not straightforward and other unknown factors, such as material properties, fault cross-cutting features, etc., may influence this or that the resolution of the falloff of slip at the fault end was still not good enough at that time.

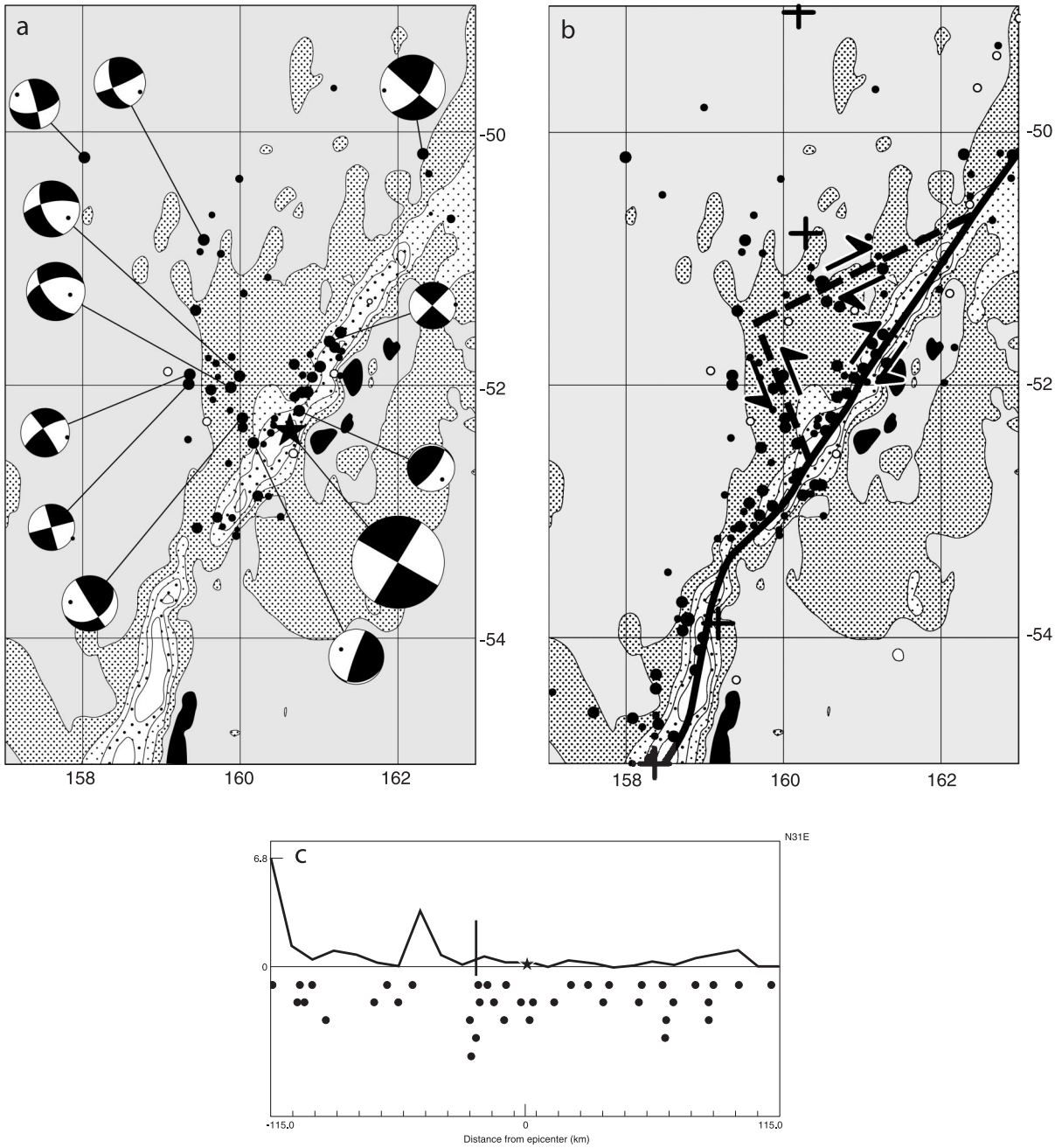


**Figure 5.** (a) Relocated aftershocks for the 7-month period following the 23 May 1989 Macquarie Ridge earthquake (with a seismic moment of $1.34 \times 10^{21}$ N m) (taken from *Das* [1993], reprinted with permission of Blackwell Publishing) and their Harvard centroid moment tensor (CMT) solutions. The 1-day and 7-day aftershocks were also plotted by *Das* [1993], and this showed that there is little difference between the 7-day and the 7-month distributions. The CMT solution for the main earthquake was obtained by *Das* [1993] and differs from the Harvard one (see *Dziewonski et al.* [1983–1999] for more details). (b) Tectonic interpretation of Macquarie Ridge earthquake (taken from *Das* [1993], reprinted with permission of Blackwell Publishing) showing the rotation of the triangular region, outlined by dashed lines and the plate boundary and with arrows indicating the sense of motion on its three sides. (c) Final moment distribution along strike for the Macquarie Ridge earthquake, compared with those aftershocks that occurred on or near the main fault. The spatial and temporal grid sizes used in the inversion for the slip were 20 km × 20 km and 5 s, respectively. In order not to hide overlapping aftershocks the aftershocks are staggered along the ordinate of Figure 5c. Most aftershocks occur north of the intersection (shown by a vertical line) with the main fault of a second fault that was reactivated following the main shock [*Das*, 1992]. Reproduced from *Das and Kostrov* [1994]. Reprinted with permission from Elsevier.

### 2.2. $M_w$ 8.1 1998 Strike-Slip Antarctic Plate Earthquake (Figure 6)

[21] The $M_w$ 8.1 1998 strike-slip Antarctic plate earthquake was the largest crustal submarine intraplate earthquake ever recorded, the largest strike-slip earthquake since 1977, and at the time the fifth largest of any type worldwide since 1977. It occurred in a region where no seismicity had previously been recorded and was the largest known on the entire Antarctic plate. Its occurrence is still puzzling as its rupture zone does not coincide with any known feature on the ocean floor, all of which are nearly N-S trending in this region. Even worse, the rupture is nearly E-W trending and actually cuts across these features at right angles. The earthquake was shown to consist of two subevents. The first subevent is a simple, primarily westward propagating ~140-km rupture, of ~45-s duration, with $M_w = 8.0$, and a stress drop of ~24 MPa, this stress drop being an order of magnitude larger than most earthquakes of this magnitude. The earthquake then jumped over a 70- to 100-km unbroken barrier and, after a time delay of ~40 s, propagated for another 60 km, resulting in a second subevent with $M_w = 7.6–7.8$, also having an unusually large stress drop. Each subevent propagated at an average speed just below the shear wave speed of the medium. This was an example of dynamic stress triggering over the largest separation distance ever found [*Henry et al.*, 2000].

[22] There were relatively few aftershocks on the bilaterally propagating main fault plane, only two in the magnitude range $5 < M_w < 6$ and large enough to have CMT solutions. No significant aftershocks occurred within the region of greatest slip nor within the unbroken barrier separating the two subevents of the earthquake. Figure 6b shows that the aftershock pattern, including all the significant clusters, was firmly established in the first 24-hour period following the main shock. *Henry et al.* [2000] showed that the first subevent was terminated at both ends by preexisting fossil fracture zones F3a and F4, and the second one terminated on F1a. The slip has a rapid falloff at both ends of the first, and larger, subearthquake. By our criterion this means that we have sharp stress concentration at both of these ends. Aftershock clusters did occur at both of these ends, confirming this identification. We conclude that for this earthquake, aftershocks occurred where there is a sharp gradient in the slip; that is, most aftershocks occurred at the edges of regions of high slip, mainly at the ends.

### 2.3. $M_w$ 7.8 2000 Strike-Slip Wharton Basin Earthquake (Figure 7a)

[23] The $M_w$ 7.8 2000 strike-slip Wharton Basin intraplate earthquake occurred in the central portion of the Indian Ocean in a place where no large earthquake has previously been recorded. The earthquake was shown to have consisted of two subevents and was remarkable in that it dynamically triggered the second rupture several seconds after the main shock initiation on a conjugate fault plane ~ 50 km to the east, resulting in a second $M_w$ 7.4 subearthquake [*Robinson et al.*, 2001]. The first rupture was ~80 km long, with ~8 m of average slip and 20 MPa of stress drop, resulting in a $M_w$ 7.8 event. The second earthquake was ~50 km long, with 3 m of average slip and 8 MPa of stress drop, being a $M_w$ 7.4 earthquake. The average rupture speeds for both subevents were about the shear wave speed of the medium, though of course the resolution for the second subevent is not as good as that for the first one. The slip distribution obtained by *Robinson et al.* [2001] shows that slip ends abruptly at the northern end of this bilaterally propagating main shock fault but has a very clear gentler falloff at the southern end. No ocean floor features give us any indication on how the earthquake terminated at either end.

[24] There are remarkably few aftershocks for such a large earthquake. Of the two large aftershocks, one occurred at the southern end of the fault, and the other occurred ~20 km beyond the northern end and farther to the north. Though aftershocks are few, there are more near the northern end. The shape of the slip distribution along the fault length suggests abrupt termination and sharp stress concentration at the northern end and dull stress concentration at the southern end; these conclusions are born out by the aftershock locations. One small aftershock occurred in the region of highest slip. The dynamic triggering of the second subearthquake on a conjugate fault is analogous to the statically triggered aftershocks on the conjugate plane to be discussed in section 4. Such coseismic rupture on conjugate faults is rare but does occur. One famous example is the 1927 Tango, Japan, earthquake (Figure 7b), discussed by *Richter* [1958]. The coseismic rupture on the two conjugate faults was determined by observers in the vicinity of the epicenter and not by a direct analysis as for the Wharton Basin earthquake. It is interesting to note that for both the 1927 and the 2000 earthquakes the two faults do not actually intersect, and there is a clear gap between the main fault and the conjugate fault rupture. Several other examples of probable conjugate fault rupturing have been listed by *Jones and Hough* [1995].

### 2.4. $M_w$ 7.3 1992 Strike-Slip Landers, California, Earthquake (Figure 8)

[25] The $M_w$ 7.3 1992 strike-slip Landers, California, earthquake is the smallest earthquake of the seven considered in detail here, but it is included because it is one of the best recorded, and as a result it is a very well studied earthquake (see the special issue of the *Bulletin of the Seismological Society of America* devoted to this earthquake, 1994). It is also the only one in this study that did not occur under water. Hence data other than seismic, for example, geological field data, geodetic data using global positioning satellite and satellite radar interferometry, were available for this earthquake, none of which are available for submarine earthquakes. The earthquake ruptured several surface-mapped fault seg-

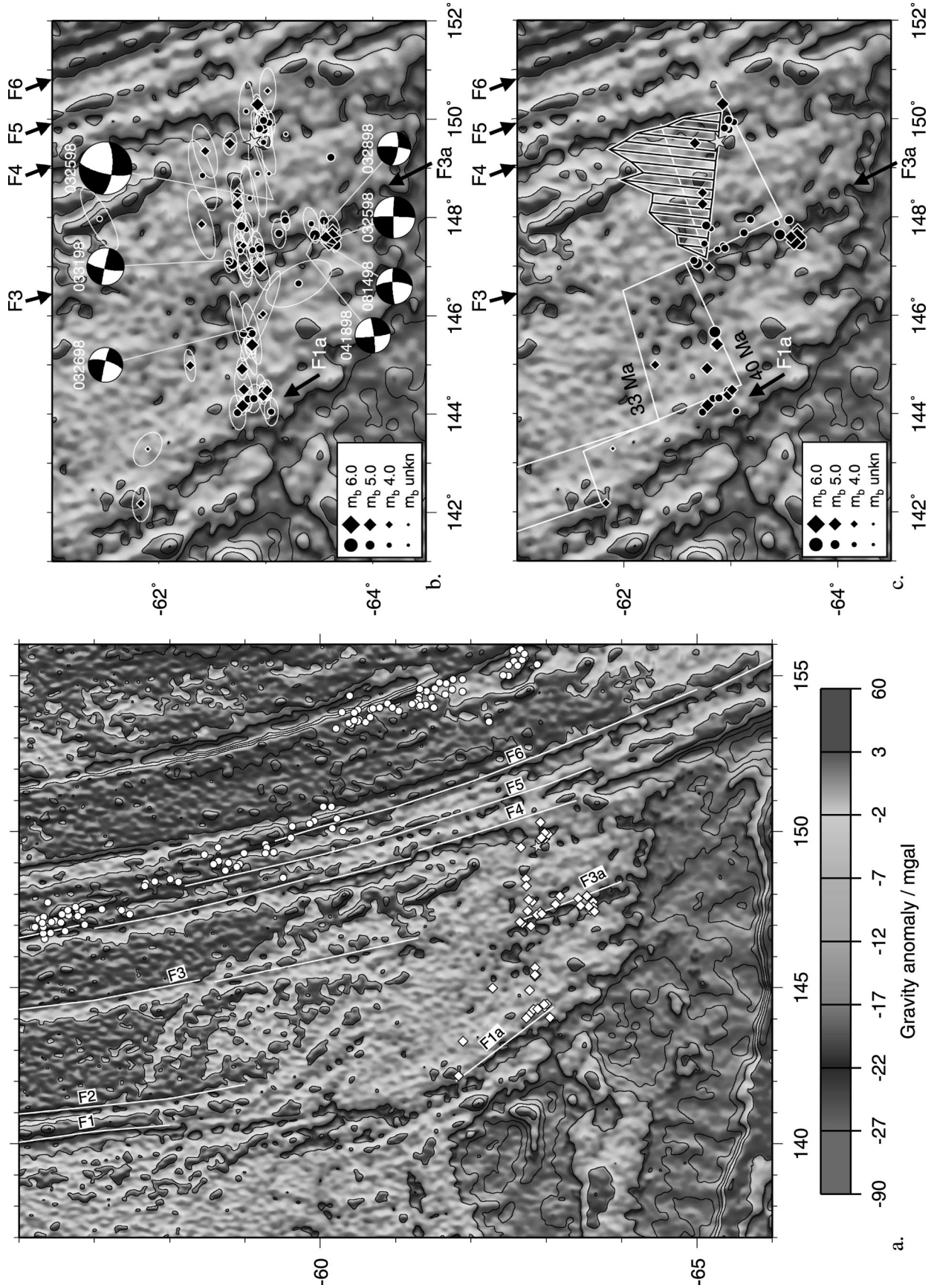
F6
F5
F4
F3
F3a
F2
F1
F1a
032598
033198
032698
041898
081498
032898
33 Ma
40 Ma
$m_b$ 6.0
$m_b$ 5.0
$m_b$ 4.0
$m_b$ unkn
Gravity anomaly / mgal
-90 -27 -22 -17 -12 -7 -2 3 60
140 145 150 155
-60 -65
142° 144° 146° 148° 150° 152°
-62° -64°
a.
b.
c.

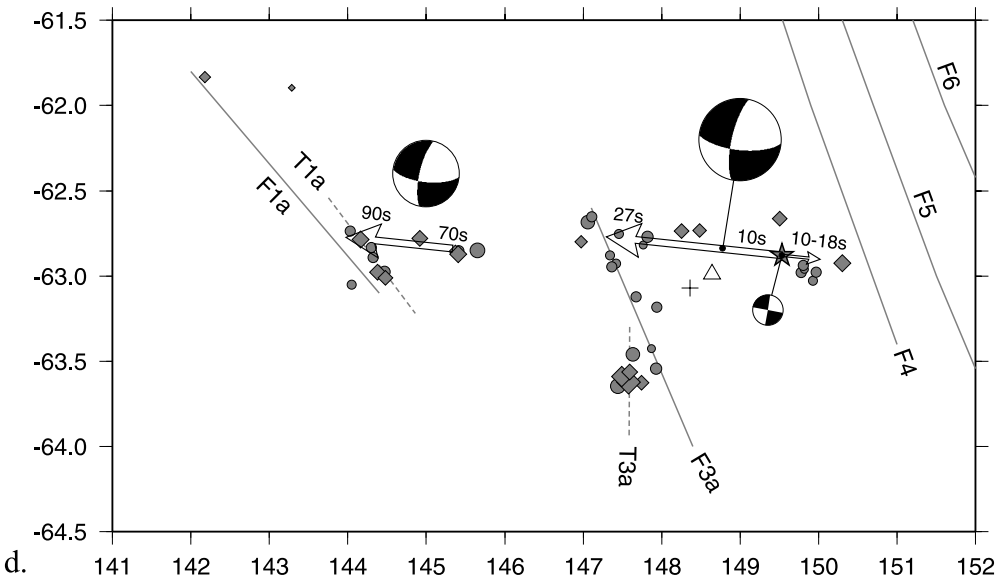


**Figure 6.** (opposite) The 25 March 1998 Antarctic plate earthquake (with a seismic moment of $1.3 \times 10^{21}$ N m). (a) Relocated aftershocks [*Henry et al.*, 2000] for the period 25 March 1998 to 25 March 1999 are shown as diamonds, with the main shock epicenter shown by a star. Only those earthquakes which are located with the semimajor axis of the 90% confidence ellipse <20 km are shown. International Seismological Centre epicenters for the period 1 January 1964 to 31 July 1997 are shown as circles. Marine gravity anomalies from an updated version of *Sandwell and Smith* [1997], illuminated from the east, with contours every 20 mGal, are shown in the background in the epicentral region. Selected linear gravity features are identified by white lines and are labeled F1–F6. F1, F2, and their southward continuation to join F1a compose the George V fracture zone. F4–F6 compose the Tasman fracture zone. (b) An expanded view of the region of the aftershocks. The relocated aftershocks in the first 24 hours are shown as diamonds; the rest are shown as circles. The 90% confidence ellipses are plotted for the locations; earthquakes without confidence ellipses were not successfully relocated and are plotted at the National Earthquake Information Center (NEIC) locations. The yellow star shows the NEIC epicenter for the main shock, with the CMT mechanism of solution 5 from *Henry et al.* [2000]. Available Harvard CMT solutions for the aftershocks are plotted, linked with lines to their centroid locations and then to their relocated epicenters, and are identified by their dates (mmddyy). The location of the linear features identified on Figure 6a are shown by black arrows. (c) Final distribution of moment release for preferred solution 8 of *Henry et al.* [2000]. There are the same gravity anomalies, same linear features, and same epicenters as Figure 6b except that now only earthquakes which are located with the semimajor axis of the 90% confidence ellipse <20 km are shown. Two isochrons from *Müller et al.* [1997] are plotted as white lines. Superimposed graph shows the final moment density, with a peak density of $1.25 \times 10^{19}$ N m km $^{-1}$. Regions of the fault with <15% of this maximum value are excluded in this plot. The baseline of the graph is the physical location of the fault. The spatial and temporal grid sizes used in the inversion for the slip were 5 km × 5 km and 3 s, respectively. (d) Principal features of the main shock rupture process [from *Henry et al.*, 2000]. Arrows show location and directivity for the first and second subevents. Arrows are labeled with start and end times of rupture segments. Focal mechanisms are shown for the initiation, the first subevent plotted at the centroid obtained by *Henry et al.* [2000], and the second subevent. (The second subevent is not well located, and the centroid location is not indicated.) The cross shows the centroid location of moment tensor of the total earthquake obtained by *Henry et al.* [2000], and the triangle shows the Harvard CMT centroid. The same aftershock epicenters as Figure 6c are shown. Linear gravity features are shown as shaded lines, and probable locations of tectonic features T1a and T3a associated with the gravity features F1a and F3a are shown as shaded dashed lines. (See *Henry et al.* [2000] for further details.) See color version of this figure at the back of this issue.

ments, the Johnson Valley, the Landers, the Homestead Valley, the Emerson, and the Camp Rock segments, listed from south to north and with the rupture propagating essentially unilaterally northward. The average rupture speed was comparable to the shear wave speed, but rupture propagation history was complex. The slip distribution was extremely nonuniform. The southernmost Johnson Valley and Landers segments had the lowest slip in the main shock [*Wald and Heaton*, 1994; *Cohee and Beroza*, 1994], and this is where the largest aftershocks occurred. The slip obtained in various studies, in which the curved fault was approximated by a plane [*Wald and Heaton*, 1994; *Cohee and Beroza*, 1994; *Madariaga et al.*, 2000] show the along-strike slip to falloff rapidly at the southern end of the entire fault, and several aftershocks are seen at this end, suggesting a

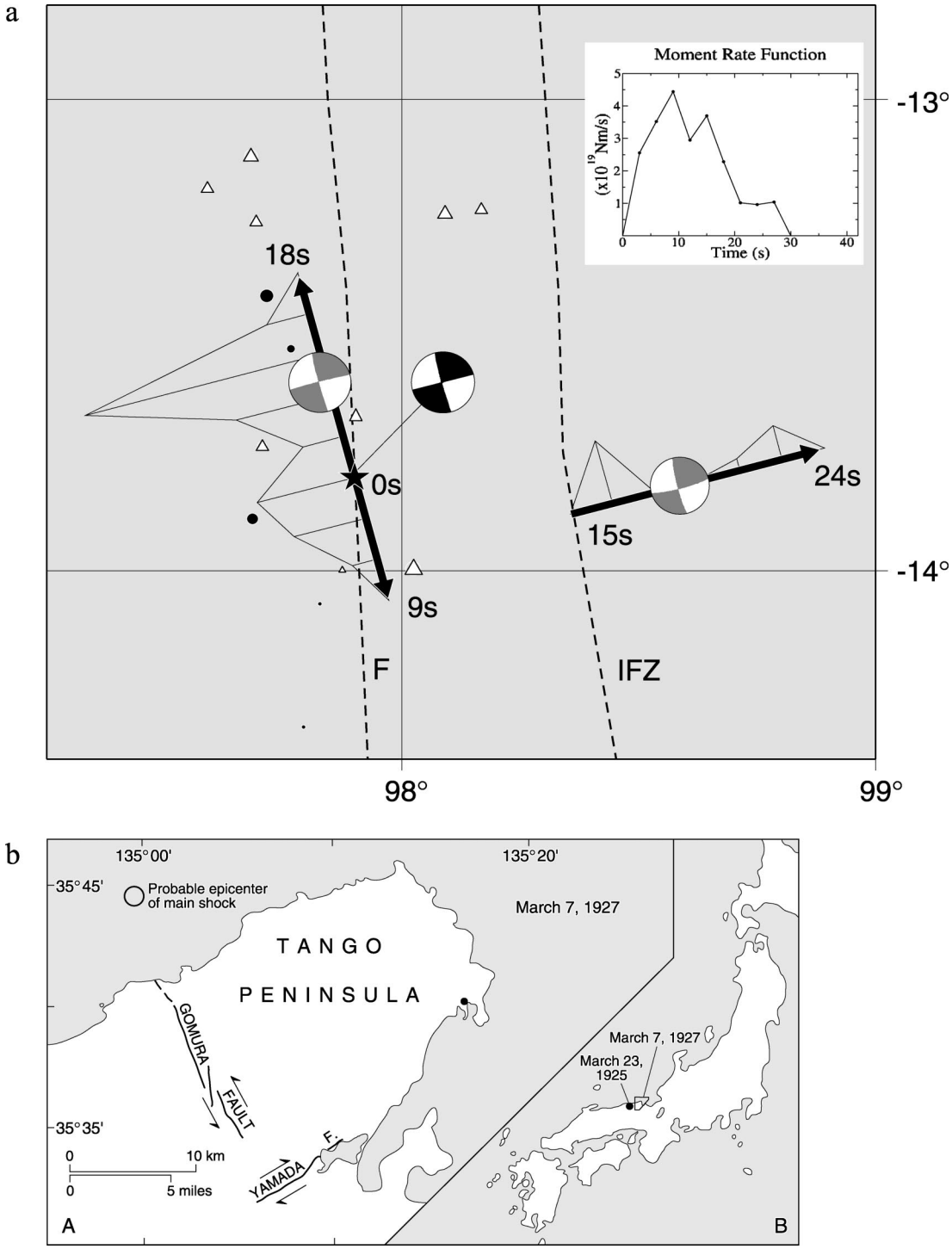


**Figure 7.** (a) Schematic showing the rupture propagation and final moment along two near-conjugate fault planes (bold solid lines) for the 18 June 2000 Wharton Basin earthquake. Reprinted with permission from *Robinson et al.* [2001] (©2001 American Association for the Advancement of Science (http://www.sciencemag.org)). The seismic moment of the earthquakes was $7.2 \times 10^{20}$ N m. The star shows the main shock epicenter and the associated CMT solution (very similar to the Harvard solution), which is the sum of the individual rupture mechanisms on the two fault planes; these are shown on the two faults. Relocated aftershocks in the 5-month period following the earthquake and with 90% confidence ellipse <30 km are shown. Circles indicate the aftershocks in the first 7 hours, and triangles indicate the rest. Regions of the fault with <10% of the maximum moment on the N-S plane are excluded in this plot. Two linear features identified from the gravity data are shown by the dashed lines, marked F and IFZ (Investigator Fracture Zone). The spatial and temporal grid sizes used in the inversion for the slip were 5 km × 5 km and 3 s, respectively. The inset shows the total moment rate function. (b) The conjugate rupture planes of the magnitude 7.3 7 March 1927 Tango, Japan, earthquake. Modified from *Richter* [1958].

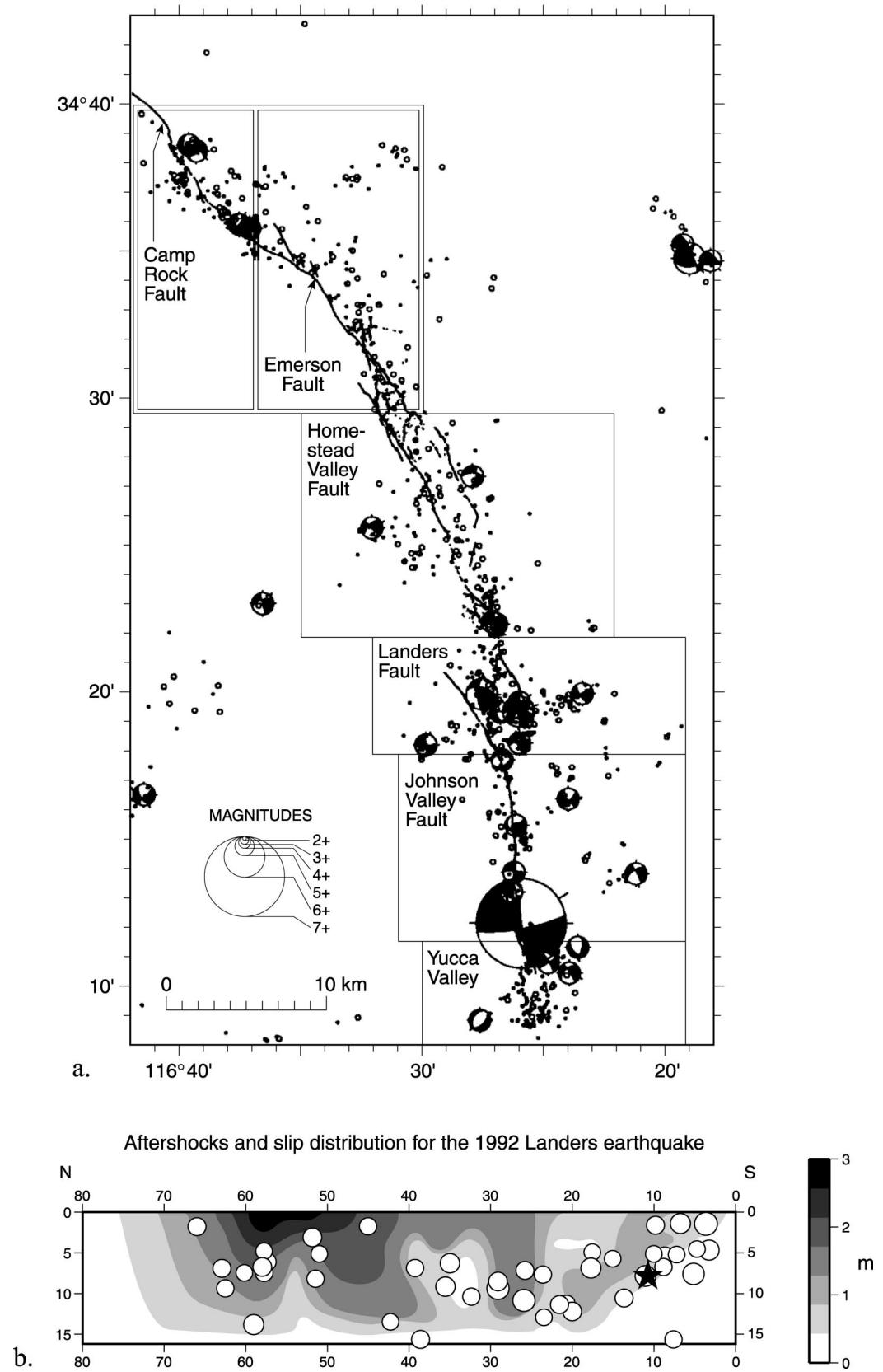


**Figure 8.** (a) Map view of the aftershock distribution of the 28 June 1992 Landers earthquake [*Hauksson*, 1994], together with available CMT solutions. The Harvard seismic moment was $1 \times 10^{20}$ N m. The largest aftershocks occur on the overlap between the Johnson Valley and the Landers segments. (b) Relocated aftershocks for the 6-month period following the earthquake, using the relocated epicenters obtained by *Hauksson* [2000], which lie <10 km from the main fault in the normal direction to it, superimposed on the fault slip distribution obtained by *Madariaga et al.* [2000]. The main shock hypocenter is indicated by the star.

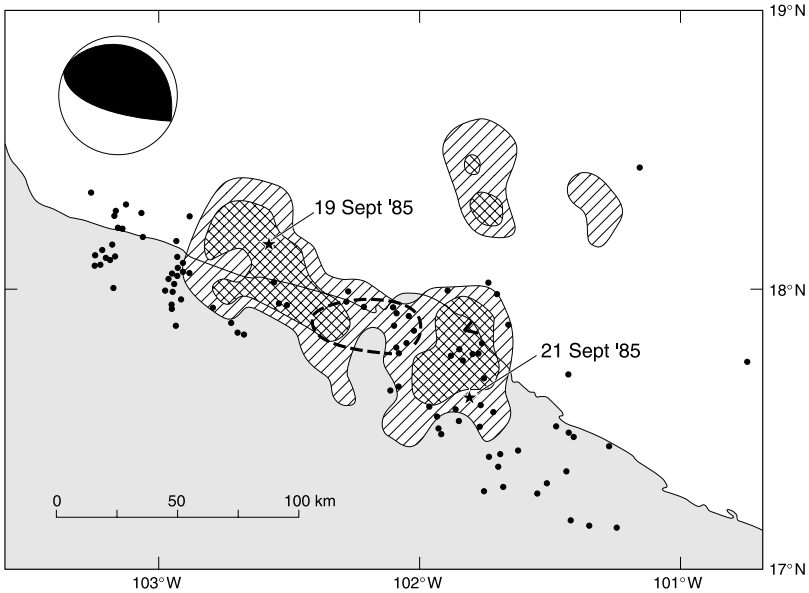


**Figure 9.** Map view of the slip distribution for the 19 September 1985 Michoacan, Mexico, earthquake [*Mendoza and Hartzell*, 1989] compared with the best located 2-week aftershocks [*Stolte et al.*, 1986]. The Harvard CMT solution is shown, the seismic moment being $1 \times 10^{21}$ N m. Areas of slip greater than 1.5 m and 2.5 m are shown by hatching and cross-hatching, respectively. The stars show the epicenters of the 19 September earthquake and its largest $M_w$ 7.5 aftershock on 21 September. Most aftershocks occur outside the regions of maximum slip, and few aftershocks occur within the aftershock area of the 1981 Playa Azul earthquake, shown by a dashed line. The spatial and temporal grid sizes used in the inversion for the slip were 15 km × 13.9 km and 2 s, respectively. (Reproduced from *Mendoza and Hartzell* [1989].)

sharp stress concentration. The slip decreases more smoothly at the northern end suggesting a weaker stress concentration there, and fewer strong aftershocks are seen at this end. The greatest concentration of aftershocks [*Hauksson*, 2000] occurs at the northern termination of these segments, where it steps over eastward on to the Homestead Valley fault (similar to the westward step over of the 1966 Parkfield earthquake). A weaker cluster of aftershocks is seen on the Camp Rock fault, which lies near the northern termination of the main shock rupture. Figure 8b clearly shows that the highest slip region is ringed by aftershocks with none within this region.

### 2.5. $M_w$ 8.0 1985 Mexico Subduction Zone Earthquake (Figure 9)

[26] The $M_w$ 8.0 1985 Mexico subduction zone thrust earthquake was located on the Cocos/North American subduction zone and is well known for having caused devastation in Mexico City, ~400 km from the epicenter, because of the resonance in the ancient sedimentary basin on which Mexico City sits. The earthquake rupture area was about 165 km long along strike and 100 km wide downdip and was one of the longest known ruptures on this plate boundary, a factor which exacerbated the damage. The slip distribution was very nonuniform, and the average rupture speed was ~70% of the local shear wave speed. The main earthquake was followed 2 days later by a $M_w$ 7.5 aftershock, located at the southern edge of the main shock fault area. Aside from this aftershock, all the others were of magnitude <5. Aftershocks occurred mainly outside the regions of maximum slip and at the two ends of the rupture, with few aftershocks in the low-slip region between two patches of high slip, which had previously ruptured in 1981 [*Mendoza and Hartzell*, 1989]. Off-fault aftershocks are seen in the wedge above the subduction zone.

### 2.6. $M_w$ 8.0 1986 Andreanof Island Subduction Zone Earthquake (Figure 10)

[27] The rupture zone of the $M_w$ 8.0 1986 Andreanof Island thrust earthquake on the Pacific/North American plate boundary was ~250 km long and was located within the ~900-km fault of the great $M_w$ 8.6 1957 Aleutian earthquake on this plate boundary. The normal repeat time of earthquakes here is ~100 years, so the occurrence of such a large earthquake so soon was unexpected and suggests that there must have been a slip deficit from the 1957 earthquake, which was being compensated in 1986. The 1986 main shock slip [*Das and Kostrov*, 1990] is compared with its aftershocks obtained from the local network data [*Ekstrom and Engdahl*, 1989] as well as with the aftershocks of the 1957 earthquake [*Boyd et al.*, 1995] in Figure 10. No clustering of aftershocks at the ends of the fault is seen for the 1986 earthquake. Unfortunately, for an earthquake in 1986 the slip is not resolved well enough to identify the shape of its falloff at the fault ends and hence to identify how the earthquake stopped. The fact that it occurred within the 1957 fault area would suggest that it propagated into

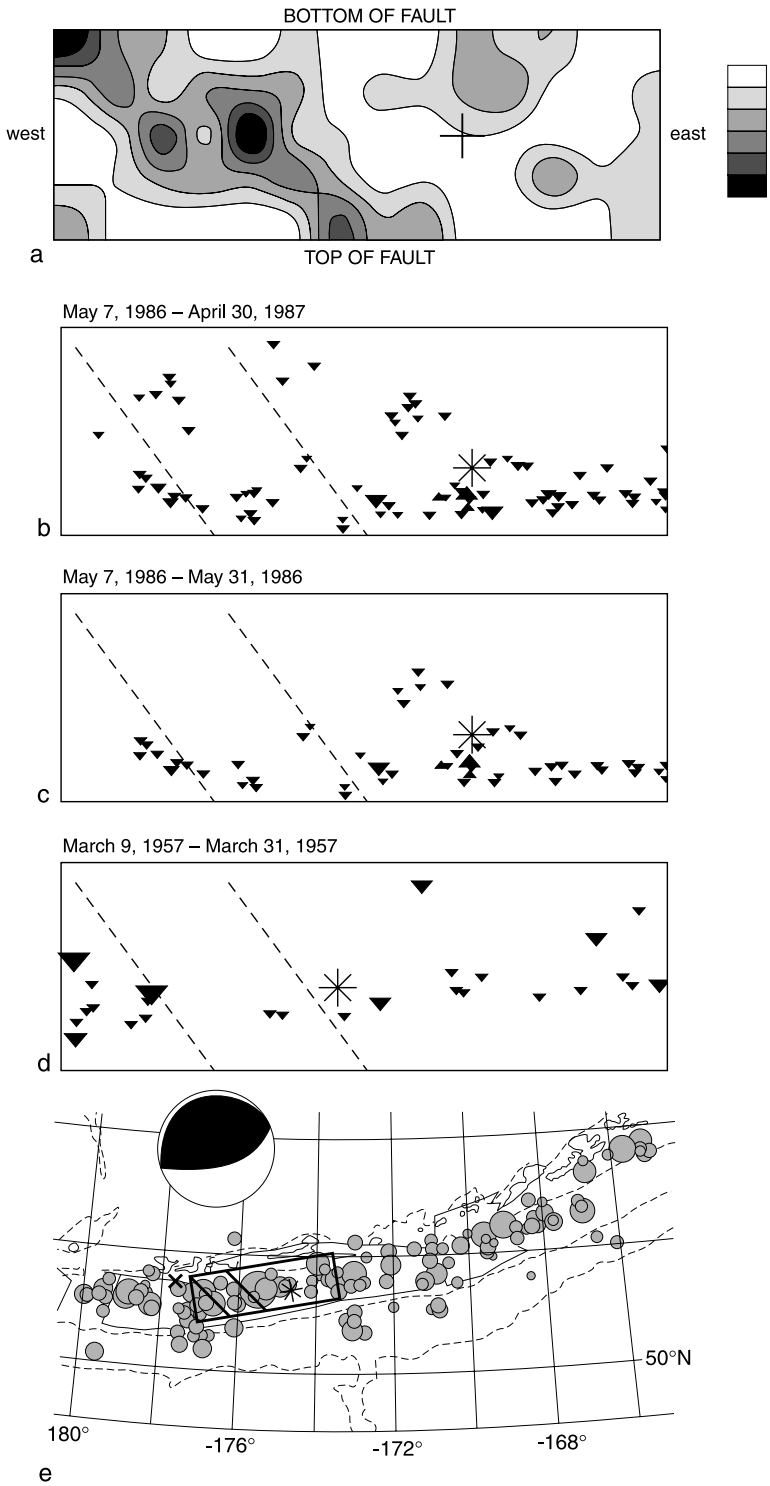


**Figure 10.** (a) Moment distribution for the 7 May 1986 Andreanof earthquake [*Das and Kostrov*, 1990], with the hypocentral cell marked by the cross. The seismic moment was $1 \times 10^{21}$ N m. The spatial and temporal grid sizes used in the inversion for the slip were 20 km × 20 km and 5 s, respectively. (b) The 1-year aftershock distribution, taken from *Ekstrom and Engdahl* [1989], projected onto the fault plane, with the region of high moment of Figure 10a indicated by the dashed lines [*Das*, 1990]. (c) Same as Figure 10b but for 3 weeks only. Figures 10b and 10c show that few aftershocks occur within the region of highest slip. (d) The 3-week aftershocks of the great 1957 Aleutian earthquake for that portion of the fault which overlaps the rupture area of the 1986 earthquake, using the data of *Engdahl et al.* [1989] (based on *Das* [1990]). (e) Map view of the 30-day aftershock distribution of the 1957 earthquake on the entire fault area, modified from *Boyd et al.* [1995]. The fault area of the 1986 earthquake and its region of high moment are shown by bold lines. The epicenter of a $M_w$ 7.9 earthquake that occurred on 10 June 1996 is shown by the cross. The Harvard CMT solution for the 1986 earthquake is shown.

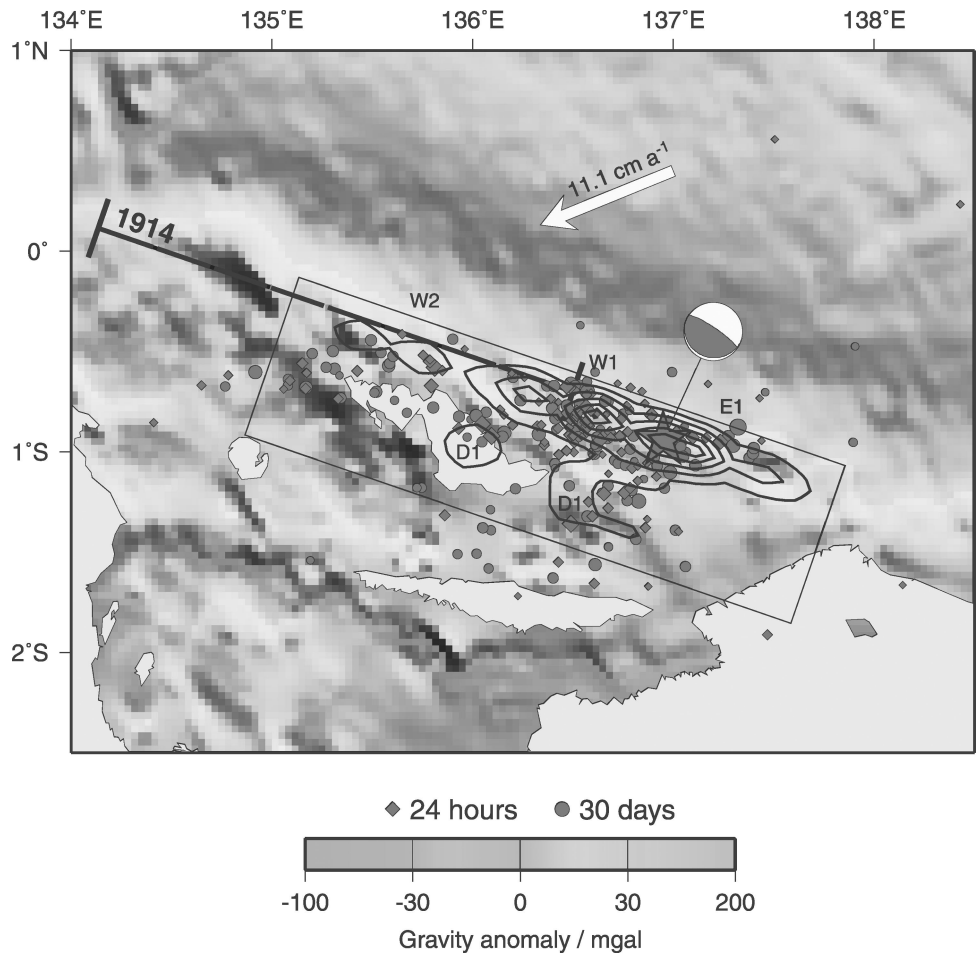


**Figure 11.** Map view of the final moment distribution for the 1996 Biak, Indonesia, earthquake and its aftershocks, together with the CMT solution for the main shock (checked by *Henry and Das* [2002] and found to be the same as the Harvard solution). The main shock epicenter is the red star. The seismic moment was $2.7 \times 10^{21}$ N m. Relocated aftershocks with 90% confidence limits (semimajor axis of error ellipse) <30 km, from 17 February 1996 to 18 March 1996, with size increasing with $m_b$ and symbol (see the key) indicating time of occurrence, are shown. The fault area is indicated by the rectangle. Solid contours at intervals of $10^{20}$ N m km$^{-2}$ show the final moment distribution. The labels W1, W2, E1, and D1 indicate features of the rupture process, with W meaning westward rupture, E meaning eastward rupture, and D meaning downward rupture and 1 and 2 indicating the first and second phases of the rupture propagation in the appropriate direction [*Henry and Das*, 2002]. Marine gravity anomaly, shown in the background, is taken from *Hwang et al.* [1998]. The NUVEL-1A Pacific-Australia plate motion vector is from *DeMets et al.* [1994]. See color version of this figure at the back of this issue.

low prestress regions and stopped. The region of high slip in this earthquake is located in an ~70-km-wide region ~160 km to the west of the hypocenter [*Das and Kostrov*, 1990; *Das*, 1990; *Das and Kostrov*, 1994], suggesting that this region did have a slip deficit from the 1957 earthquake. This same region also had few aftershocks in 1986, implying that it broke completely in 1986. However, the high-slip region of 1986, which is the region of slip deficit in 1957, only had a few small aftershocks in 1957; this difference in behavior was pointed out by *Boyd et al.* [1995]. At first, this seems not to agree with the usual observation that aftershocks concentrate in regions of low slip in the main shock. However, if this region had been a very strong, locked zone in 1957 with no slip on it at all, no aftershocks would be expected on it, a property also noted in section 2.2 regarding the lack of aftershocks on the unbroken barrier of the 1998 Antarctic earthquake. Farther to the west, the epicenter of a $M_w$ 7.9 earthquake in 1996 lies on the eastern edge of a region which had no aftershocks in 1957 (Figure 10). *Kisslinger and Kikuchi* [1997] showed that the 1996 earthquake propagated primarily westward into this region, and thus the 1996 earthquake may represent the rupture of a second region with slip deficit from 1957. This region had many aftershocks in 1996 [*Kisslinger and Kikuchi*, 1997], so the 1986 and 1996 earthquakes in spite of both being slip-deficit compensating earthquakes of the 1957 event are not similar in this respect. It is interesting to note that the 1986 earthquake was nearly correctly predicted by *Kisslinger* [1988]

**Table 1. Summary of Locations Where Aftershocks Do and Do Not Occur**

| *Location* | *Examples* |
|---|---|
| | *Locations Where Aftershocks Occur* |
| Main shock slip | |
| Terminations | 1984 Morgan Hill, 1985 Mexico, 1986 North Palm Springs, 1992 Landers, 1995 Chile, 1998 Antarctic plate, 2000 Wharton Basin |
| Transition from high to low slip | 1989 Macquarie, 1992 Landers |
| Edge of unbroken barrier | 1998 Antarctic plate |
| Low-slip regions | 1979 Imperial Valley, 1989 Macquarie Ridge, 1992 Landers |
| Main shock geometry | |
| Step overs | 1992 Landers |
| Change in strike | 1992 Landers |
| Intersections with other faults | 1989 Macquarie |
| Off-fault locations | |
| Tectonic features | 1989 Macquarie Ridge, 1992 Landers, 1998 Antarctic plate |
| Concave side of curved main fault | 1992 Landers |
| | *Locations Where Aftershocks Do Not Occur* |
| Main shock slip | |
| Regions of high slip | 1979 Imperial Valley, 1983 Borah Peak, 1984 Morgan Hill, 1985 Mexico, 1986 Andreanof, 1986 North Palm Springs, 1989 Macquarie Ridge, 1992 Landers, 1998 Antarctic plate, 2000 Wharton Basin |
| High slip in previous earthquake | 1985 Mexico |
| Large unbroken barriers | 1998 Antarctic, 1957 Aleutian |
| Off-fault locations | |
| Region without favorable weak planes | 1989 Macquarie Ridge, 1998 Antarctic plate |
| Convex side of curved main fault | 1992 Landers |

from observed seismic quiescence before the earthquake; he gave a time window, magnitude, and expected direction of rupture propagation. The earthquake occurred later than predicted, was much larger than predicted, did not nucleate in the expected region but ~90 km to the east, and the rupture direction was not correct. However, the region of high slip in the 1986 earthquake coincides with the region of the seismic quiescence, suggesting that the quiescence may have been indicative of high slip rather than rupture nucleation position. Small off-fault aftershocks occur in the wedge above the subduction zone.

### 2.7. $M_w$ 8.2 1996 Biak, Indonesia, Subduction Zone Earthquake (Figure 11)

[28] The occurrence of the $M_w$ 8.2 1996 Biak, Indonesia, earthquake, the largest thrust earthquake at its time worldwide since 1977 and the second largest from 1977 to 2002, within a part of the New Guinea Trench on the Australia/Pacific plate boundary previously considered aseismic showed that the trench is active and has great earthquakes. The rupture propagated bilaterally at an average speed of ~90% of the shear wave speed on a fault extending 180 km west and 50 km east of the hypocenter, with very variable width ranging from 30 to 100 km at different locations along strike. The mean slip over a 230 × 100 km fault area was 4 m, and the mean stress drop was 1.9 MPa. The slip distribution was shown to be very nonuniform over the fault, and the rupture process was shown to be very complex, propagating first to the west and then, after a clear delay, to the east [*Henry and Das*, 2002].

[29] Figure 11 shows that the overall pattern of aftershocks was established in the first 24 hours following the main shock, with a very slight expansion to the east in the following 30-day period. The aftershock zone closely corresponds to the region in which rupture occurred, with the greatest aftershock density lying entirely within the area of highest moment. This is the only earthquake of the seven being discussed in detail for which we have observed such a correlation. The strongest cluster of aftershocks (i.e., the region with many aftershocks including the larger ones) lies in the center of the rupture propagating west from the hypocenter and is labeled W1 in Figure 11. *Henry and Das* [2002] and *Henry* [2002] carried out a very detailed investigation of the range of slip distributions consistent with the body wave data and found that this cluster of aftershocks occurs either at the spatial maximum of seismic moment or on a transition region from high to medium moment. A strong, inhomogeneous barrier was identified extending east from the hypocenter, this barrier being the initiator of rupture, having foreshocks on it, and delaying rupture propagation (E1 in Figure 11) to the east by ~15 s after the origin time [*Henry and Das*, 2002]. The aftershocks have been examined in cross section (not shown), and all the well-located ones occur very close to the main fault plane. However, some off-fault aftershocks do seem to occur, though we cannot identify which ones they are.

Some of these aftershocks have CMT solutions with normal or strike-slip mechanisms.

### 2.8. Several Earthquakes From the Western United States

[30] In addition to the seven recent large earthquakes discussed in sections 2.1–2.7, we also consider six moderate to large earthquakes ($6 \leq M_w \leq 7$) analyzed in sufficient detail for the purpose of this study, for which the slip distributions were obtained by a formal inversion of the seismograms. Four earthquakes between 1979 and 1986 were studied by *Mendoza and Hartzell* [1988a]. For the $M_w$ 6.5 1979 strike-slip Imperial Valley, California, earthquake most aftershocks occurred on a long segment of the fault northwest of the area with large moment in the main shock, with few aftershocks within the main area of slip. The aftershocks of the $M_w$ 6.1 1984 Morgan Hill, California, and the $M_w$ 6.0 1986 North Palm Springs, California, strike-slip earthquakes also primarily occur on the edges of regions of high slip with very few aftershocks in the regions of high moment. For the $M_w$ 6.9 1983 dip-slip Borah Peak, Idaho, earthquake the aftershocks mostly occur within a narrow depth range dividing a deep and a shallow region of high slip. On this basis, *Mendoza and Hartzell* [1988a] concluded that most aftershocks occur at the edges of regions of high slip or in regions of low slip, and they interpreted these as being consistent with the hypothesis that aftershocks occur in regions that have high stress following the occurrence of the main shock. *Hartzell et al.* [1991] studied the $M_w$ 7.0 1989 dip-slip Loma Prieta, California, earthquake and found that "most aftershocks plot within the boundaries of the region of major slip." For the $M_w$ 6.7 17 January 1994 Northridge, California, earthquake the aftershocks clustered on regions of high-slip gradients, and the largest aftershock occurred in a region of low slip [*Wald et al.*, 1996]. Some older, smaller, earthquakes for which similar comparisons of slip and aftershock have been made have been discussed by *Mendoza and Hartzell* [1988a] and by *Oppenheimer et al.* [1990], and they reached the general conclusion that the low-slip regions have more numerous aftershocks.

## 3. WHERE THE AFTERSHOCKS ON OR NEAR THE MAIN RUPTURE LIE RELATIVE TO THE MAIN SHOCK SLIP

[31] The aftershocks discussed up to now that occur on or near the main fault plane are located in regions of increased stress due to the main earthquake. Aside from this common feature, no single simple relationship can explain all their locations. The different factors that can lead to the occurrence of near-fault aftershocks are summarized in Table 1, with specific examples of relevant earthquakes for each scenario. The most consistent observation is that few aftershocks occur in the region of highest slip, which is generally closely allied with the region of high stress drop, and we shall refer to such high-slip regions as "asperities" from now on. The great 1996 Biak earthquake is the only exception, with many large aftershocks occurring in the region of high slip. We interpret this general observation that few aftershocks occur in high-slip regions as implying that the asperities generally break completely and thus have low slip and hence low stress gradients. The 1985 Mexico earthquake had relatively few aftershocks in the regions of high slip, but the fact that it also had few aftershocks in the central shallow region of very low slip can be explained as being due to the occurrence of the Playa Azul earthquake in 1981 in this region of low slip. Thus our earlier statement that few aftershocks occur in regions of high slip could be modified to say few aftershocks occur in regions of cumulative recent high slip. This general relation, however, is based on models of planar faults and with no cross-cutting features across the fault. In complex tectonic regions both of these could exist, and one can speculate along these lines why the 1996 Biak earthquake or portions of the 1957 Aleutians rupture zone do not fit the pattern.

**Table 2. Summary of Examples of Barriers**

| *Earthquake* | *Location* |
|---|---|
| | *Geometric Barrier* |
| 1989 Macquarie | southern end (sharp stress concentrator) |
| | *Inhomogeneous Barrier* |
| 1989 Macquarie | northern end (dull stress concentrator) |
| 1992 Landers | north (sharp) and south (duller) |
| 1996 Biak | east of hypocenter, barrier which delayed eastward propagation by 15 s (dull at both ends) |
| 1998 Antarctic plate | first subevent both ends terminated by preexisting fracture zones (sharp), 70-100 km barrier on western side |
| 2000 Wharton | (dull) |

[32] Though there are generally fewer aftershocks in regions of high slip, the reverse is not always true; that is, we do not always see more aftershocks in the low-slip regions. This could be understood as follows. If we could always distinguish between regions on the fault where there is little slip, say, because of a lack of stress accumulation there due to recent previous slip, from very strong, completely locked zones with no slip at all, we could expect the former to have some aftershocks but the latter to have none at all. Thus small unbroken barriers can have aftershock concentrations, but very large unbroken barriers would generally have aftershocks at its edges only. The 1966 Parkfield earthquake would be an example of the former, and the 1998 Antarctic and the 1957 Aleutian earthquakes are examples of the latter.

[33] For most earthquakes, aftershocks are seen at both terminations of the rupture, but some earthquakes only have aftershocks at one end, and some have no

**Table 3. Location of Rupture Nucleation Relative to High and Low Slip**

| *Slip at Hypocenter* | *Earthquake* |
|---|---|
| Low | 1983 Borah Peak |
| | 1984 Morgan Hill |
| | 1985 Mexico |
| | 1986 Andreanof |
| | 1989 Macquarie |
| | 1992 Landers |
| Modest | 1979 Imperial Valley |
| High | 1986 Palm Springs |
| | 1998 Antarctic |
| | 1998 Biak |
| | 2000 Wharton |

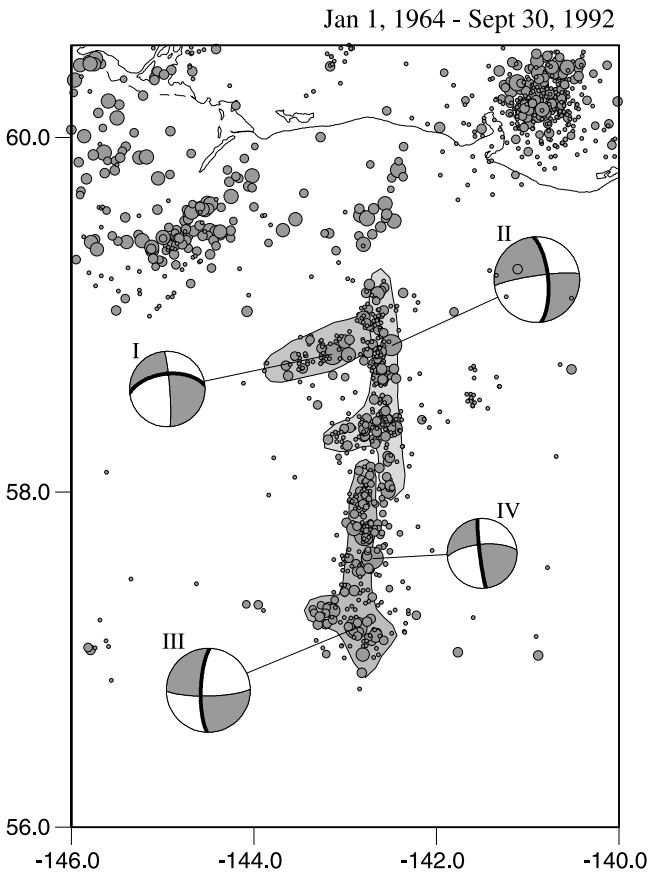


**Figure 12.** The relocated aftershocks and the Harvard CMT solutions for the 1987–1992 Gulf of Alaska sequence of earthquakes. Earthquake I occurred on 17 November 1987 ($M_w$ 7.2); earthquake II occurred on 30 November 1987 ($M_w$ 7.8); earthquake III occurred on 6 March 1988 ($M_w$ 7.7); earthquake IV occurred more than 4 years later on 7 August 1992 ($M_w$ 6.8). Relocated aftershocks for the period 17 November 1987 to 30 September 1992 are taken from *Pegler and Das* [1996b]; the aftershock distributions for shorter periods following each earthquake of the sequence are also shown in that paper. The rupture plane of each earthquake, identified by *Pegler and Das* [1996b], is indicated on the CMT solution by the bold line.

clustering at all at the ends. The 1989 Macquarie Ridge earthquake is an example of the latter, though the largest aftershock is near the southern end where the plate boundary changes direction. *Das* [1992] identified the termination of this earthquake at the southern end as being due to this geometrical barrier. Whether or not aftershocks cluster at the ends of faults may depend on the sharpness of the rupture termination resulting in sharp and dull stress concentrators. Of the earthquakes looked at here, the slip distributions for only the four most recent, namely, the 1992 Landers, the 1996 Biak, the 1998 Antarctic, and the 2000 Wharton Basin earthquakes have been determined with sufficient precision to address this question. The results are summarized in Table 2.

[34] For some earthquakes, clusters of aftershocks are also seen at the transitions between high- and low-slip areas of the fault, similar to the earlier observation of *Mendoza and Hartzell* [1988a]. The earthquakes considered in detail here generally show agreement with their conclusion that aftershocks occur in regions of low cumulative slip or at edges of high-slip zones (which are obviously regions of increased stress).

[35] As quoted earlier, *Aki* [1979] suggested that we should expect many aftershocks on low-slip regions. In general, we do find this, the extreme cases being the concentration of aftershocks on unbroken barriers. For the 1966 $M_w$ strike-slip Parkfield earthquake, *Aki* [1979] showed that the largest concentration of aftershocks occurred on the 3-km step over of the fault near the southern end of the fault (Figure 3) and interpreted this step over as an unbroken barrier near station 2 that was jumped over by the earthquake. We do not regard the lack of aftershocks on the 70- to 100-km barrier of the 1998 Antarctic earthquake as being in conflict with the idea that aftershocks concentrate on unbroken barriers, because close examination of Figure 6 shows that some aftershocks do occur at the edges of this barrier. The lack of aftershocks in the interior of the barrier implies that the stress concentrations localized at the edges of the barrier, as expected, and the interior of the barrier was too strong to have aftershocks. Remember that this was a barrier strong enough to have stopped a magnitude 8 earthquake, the westward propagating first subevent of the 1998 Antarctic earthquake.

[36] From the detailed study of the slip distribution of the 1986 Andreanof Islands earthquake, coupled with the seismicity following the 1957 Aleutian earthquake (Figure 10), it is possible to identify a region of little or no slip in the 1957 earthquake, which is the region of high moment in the 1986 earthquake, even though detailed slip distributions cannot be obtained for earthquakes that occurred so long ago. The lack of aftershocks on this zone in 1957 suggests that this may have actually been a strong locked region in 1957.

[37] Finally, we examine whether the nucleation region of an earthquake lies in the region of high or low slip. The information is summarized in Table 3 and

shows that no simple relation exists and that earthquakes can originate in high- or low-moment regions.

## 4. OFF-FAULT AFTERSHOCKS

[38] *Smith and Van de Lindt* [1969] suggested that the off-fault aftershocks of the 1968 Borrego Mountain, California, earthquake were due to increased stresses there. Since this stress increase was based on *Chinnery*'s [1963] theoretical "dislocation" model with a constant displacement over the entire fault and since it is well known that such a model leads to unrealistic stresses at some parts of the fault, namely, the edges, it was not clear if the off-fault stress increase was realistic, and their suggestion was ignored. It is only when *Kostrov and Das* [1982] showed that such off-fault increases also occur for theoretical shear "crack" models with constant stress drops on the fault and laboratory experiments confirmed this [*Gzovsky et al.*, 1974; *Osokina and Tsvetkova*, 1979] that the occurrence of this off-fault stress increase was accepted. It is interesting to note that this off-fault stress increase exists for the two-dimensional (2-D) in-plane shear fault as well as for all 3-D faults but not for the 2-D antiplane shear case [*Kostrov and Das*, 1984]. When, using this result, *Das and Scholz* [1981] interpreted off-fault aftershocks as being due to off-fault stress increase, *Smith and Van de Lindt*'s [1969] idea was finally accepted.

[39] Since immediately adjacent to the main shock fault the stress is reduced, off-fault aftershocks are usually spatially clearly separated from aftershocks directly associated with the main fault. This can be very clearly seen in Figure 1 and for strike-slip earthquakes with nearly vertical rupture planes. In fact, this very useful feature can be used to identify the fault plane from the two nodal planes for earthquakes when the data required to identify it from seismogram analysis are not available. It was one of the factors used by *Pegler and Das* [1996b] to identify correctly the fault plane of a $M_w$ 7.8 earthquake in the Gulf of Alaska in 1987 and for which the rupture plane was difficult to identify based on body wave modeling because of the very poor azimuthal distribution of seismic stations at the time. In fact, a sequence of four earthquakes in the Gulf of Alaska between 1987 and 1992, three very closely spaced in time, and of which the 1987 $M_w$ 7.8 was one, provides a good example of how earthquakes rupture preexisting parallel and perpendicular weak zones. The earthquakes are shown in Figure 12, details of their dates and sizes are given in the Figure 12 caption. All four were strike-slip earthquakes. The first earthquake ruptured on the E-W nodal plane; the remaining three ruptured on the N-S planes. The E-W fault was interpreted as a fossil fracture, and the N-S faults were interpreted by *Pegler and Das* [1996b] as the ridge fabric corresponding to magnetic anomaly 13. The N-S sequence terminates at the southern end on a seamount, which can be interpreted as being an inhomogeneous barrier. At the northern end the aftershocks terminate on the Alaska trench near the Yakataga seismic gap. For subduction zone earthquakes with dipping rupture planes the gap between the main fault and the region of off-fault aftershocks is less clear as identification of this separation depends strongly on obtaining the depth of the earthquake very accurately. Since these off-fault aftershocks are usually small, their error ellipses are often such that one cannot absolutely state whether the aftershock is on the main fault or not; our study of the 1996 Biak earthquake is such an example. What is clear is that large subduction zone earthquakes have many aftershocks in the triangular wedge in the hanging wall, some of which are clearly off the main fault.

[40] The off-fault stress increase is very small being at most only a few percent of the main shock stress drop [*Kostrov and Das*, 1982]. Hence it can only trigger aftershocks if there are preexisting favorably oriented weak planes close to failure located in the regions of off-fault stress increase. If weak planes exist throughout the region surrounding the rupture, then the distribution of aftershocks would be controlled by stress alone, and one would expect to see the same symmetry in their distribution on the two sides of a plane fault as exists for the stress change and as was seen, for example, for the 1972 Managua earthquake (Figure 1). For the 1989 Macquarie Ridge earthquake and the 1998 Antarctic plate earthquake, off-fault aftershocks occur only on one side of the fault plane, and on the basis of the known marine geophysics of the region this was interpreted in each case to be due to the differences in the ocean floor properties on the two sides of the fault resulting from major differences in the tectonic history of the fault formation. Aftershocks were triggered as far as 200 km away from the main shock in the off-fault region for the Macquarie Ridge earthquake (Figure 5a), which is quite unusual, and was shown by *Das* [1993] to be due to the reactivation of an old fossil fault, emplaced at the time of seafloor spreading in this region. For the 1992 Landers earthquake a large off-fault aftershock, the Big Bear earthquake, occurred on the concave side of the curved main shock fault with few aftershocks on the convex side. *King et al.* [1994] have argued qualitatively that fault curvature contributed to a larger stress increase on the concave side because of overlap of regions of stress increase.

[41] *Das and Scholz* [1981] mentioned the possibility that the rupture plane of off-fault aftershocks could be either parallel to the main shock fault or its conjugate. Which one actually ruptures in the aftershock depends on which nodal plane is weaker. Since such aftershocks are usually small, their rupture planes cannot be easily identified by analyzing seismograms. If they occur on or near some clearly visible plane of weakness, a reliable guess can be made. For example, one of the nodal planes of the off-fault aftershocks of the 1998 Antarctic earthquake aligns with a N-S trending feature on the ocean

floor, which is conjugate to the E-W trending main shock fault. In one case, field observations in the region of the off-fault aftershocks suggested rupture on the conjugate nodal plane [*Yamashina*, 1980]. However, two recent earthquakes clearly show the off-fault shock rupture plane being conjugate to that for the main shock. One is the 2000 Wharton Basin earthquake [*Robinson et al.*, 2001], in which a second rupture was triggered coseismically on a plane conjugate to the main fault and 50 km away from it, as discussed in section 2.3. The other even more complex case is the Big Bear aftershock of the 1992 Landers, California, earthquake, which has the same focal mechanism as the main shock, and it appears that the Big Bear earthquake ruptured not only the plane conjugate to the Landers rupture but that some rupture was also required on the plane parallel to the Landers fault to better fit the seismograms [*Jones and Hough*, 1995].

## 5. DISCUSSION AND CONCLUSIONS

[42] Reliable aftershock locations have been available worldwide since the mid-1960s because of the wide international deployment of seismometers. The results were used for many decades to estimate the fault rupture area, and this, in turn, was applied to many problems of interest in seismology, such as laws of scaling between small and large earthquakes and whether rupture zones of large earthquakes overlap one another at the edges or abut one another. Information on the spatial distribution of fault slip for large earthquakes, on the other hand, has become available only since the late 1980s, with the era of global digital broadband high-quality seismic instruments and the availability of the large, fast computers needed to analyze the seismograms. Only now, have we accumulated enough data on the spatial distribution of the main shock fault slip to examine where the aftershocks occur relative to it.

[43] We examine these distributions and do not find any universal relation between regions of high and low slip and aftershock occurrence. We do find that regions of high slip have fewer and smaller aftershocks for all but one of the earthquakes examined, the great 1996 Biak, Indonesia, earthquake is the exception. Regions at the edges of faults where stress is increased due to the earthquake usually, but not always, have clusters of aftershocks. Less slipped parts of faults as well as regions of sharp changes from high to low slip in the interior of the rupture area also often have aftershocks.

[44] In his paper on the character of barriers to earthquake rupture, *Aki* [1979] expected regions of smooth slip to have few aftershocks, which is not necessarily the same as regions of high slip. The exception of the Biak earthquake is interpreted by us to represent just such a situation, namely, that the region of high slip did not break smoothly and many aftershocks resulted in that region. One can speculate that the roughness of the subducting seafloor, with its seamounts and features normal to the island arc, introduces an additional element of complexity into the problem, making it more difficult to find a simple relation between slip and aftershock distribution for the 1996 Biak type of earthquake. Lack of even more detailed resolution of the slip does not allow us to obtain even finer details of the variation of the slip within the region of high slip and is an example of the limitation mentioned in section 1. The 1985 Mexico earthquake had few aftershocks in the regions of high slip as well as in a region of low slip, which had ruptured in 1981 in an earthquake. Thus we conclude that it is the recent cumulative high-slip regions that generally have fewer aftershocks. We also find that aftershocks that occur on or very near the main rupture plane are located in regions of high-slip gradient, that is, in regions with high postseismic stress. These can be regions that broke incompletely or not at all (barrier) in the main shock.

[45] An interesting question is whether there are any obvious differences between the aftershocks of oceanic and continental earthquakes. *Henry and Das* [2001] searched for this in their study of aftershocks but did not find any obvious distinction between them. What they did find was that subduction zone earthquakes have larger and more numerous aftershocks (when a consistent magnitude threshold is applied), and these aftershocks continue for much longer than those for all other types of earthquakes. No distinction was found between nonsubduction interplate and intraplate earthquakes nor between nonsubduction oceanic and continental earthquakes, nor between nonsubduction dip-slip and strike-slip earthquakes.

[46] Off-fault aftershocks occur only when there are preexisting planes of weakness within the regions of off-fault stress increase, and rupture may occur on either nodal plane. With today's high-quality seismic instruments and their dense distribution, identification of the rupture plane of larger off-fault aftershocks will become more and more common, and it will be interesting to see in the future how often such aftershocks rupture the conjugate plane.

[47] Just as regions with many faults but very low tectonic stress have few or no earthquakes, so regions of high stress but without faults are unlikely to have earthquakes. So, in summary, we conclude that aftershocks occur in regions of increased stress due to the main shock, both close to the main fault as well as in off-fault locations, provided that there are preexisting optimally oriented weak planes in these regions for the aftershocks to rupture on.

[48] **ACKNOWLEDGMENTS.** We would like to thank Egill Hauksson for giving us his relocated aftershock data for the 1992 Landers earthquake and Raul Madariaga for the use of his slip distribution for this earthquake. C. H. was supported by the U.K. NERC studentship GT04/97/ES/217 and a Schlum-

berger CASE award.

[49] Louise Kellogg was the Editor responsible for this paper. She thanks one technical reviewer and one cross-disciplinary reviewer.

## REFERENCES

Aki, K., Characterization of barriers on an earthquake fault, *J. Geophys. Res.*, *84*, 6140–6148, 1979.

Benioff, H., Mechanism and strain characteristics of the White Wolf Fault as indicated by the aftershock sequence, in *Earthquakes in Kern County, California During 1952*, Bull. Calif. Div. Mines Geol., *171*, 199–202, 1955.

Boyd, T. M., E. R. Engdahl, and W. Spencer, Seismic cycles along the Aleutian arc: Analysis of seismicity from 1957 through 1991, *J. Geophys. Res.*, *100*, 621–644, 1995.

Brown, R. D., P. L. Ward, and G. Plafker, Geologic and seismologic aspects of the Managua, Nicaragua, earthquakes of December 23, 1972, *U.S. Geol. Surv. Prof. Pap.*, *838*, 34 pp., 1973.

Chinnery, M. A., The stress changes that accompany strike-slip faulting, *Bull. Seismol. Soc., Am.*, *53*, 921–932, 1963.

Cochard, A., and R. Madariaga, Dynamic faulting under rate-dependent friction, *Pure Appl. Geophys.*, *142*, 419–445, 1994.

Cochard, A., and R. Madariaga, Complexity of seismicity due to highly rate-dependent friction, *J. Geophys. Res.*, *101*, 25,321–25,336, 1996.

Cohee, B. P., and G. C. Beroza, Slip distribution of the 1992 Landers earthquake and its implications for earthquake source mechanics, *Bull. Seismol. Soc. Am.*, *84*, 692–712, 1994.

Das, S., A numerical study of rupture propagation and earthquake source mechanism, Sc.D. thesis, Mass. Inst. of Technol., Cambridge, 1976.

Das, S., Tectonic implications of the moment distribution of the 1986 Andreanof Islands earthquake, in *International Symposium on Earthquake Source Physics and Earthquake Precursors (Extended Abstracts)*, pp. 143–146, Univ. of Tokyo Press, Tokyo, 1990.

Das, S., Reactivation of an oceanic fracture by the Macquarie Ridge earthquake of 1989, *Nature*, *357*, 150–153, 1992.

Das, S., The Macquarie Ridge earthquake of 1989, *Geophys. J. Int.*, *115*, 778–798, 1993.

Das, S., and K. Aki, Fault plane with barriers: A versatile earthquake model, *J. Geophys. Res.*, *82*, 5658–5670, 1977.

Das, S., and B. V. Kostrov, An investigation of the complexity of the earthquake source time function using dynamic faulting models, *J. Geophys. Res.*, *93*, 8035–8050, 1988.

Das, S., and B. V. Kostrov, Inversion for seismic slip rate and distribution with stabilizing constraints: Application to the 1986 Andreanof Islands earthquake, *J. Geophys. Res.*, *95*, 6899–6913, 1990.

Das, S., and B. V. Kostrov, Diversity of solutions of the problem of earthquake faulting inversion: Application to *SH* waves for the great 1989 Macquarie Ridge earthquake, *Phys. Earth Planet. Inter., 85*, 293–318, 1994.

Das, S., and C. Scholz, Off-fault aftershock clusters caused by shear stress increase?, *Bull. Seismol. Soc. Am.*, *71*, 1669–1675, 1981.

Das, S., P. Suhadolc, and B. V. Kostrov, Realistic inversions to obtain gross properties of the earthquake faulting process, *Tectonophysics*, *261*, 165–177, 1996.

DeMets, C., R. G. Gordon, D. F. Argus, and S. Stein, Effect of recent revisions to the geomagnetic reversal time scale on estimate of current plate motions, *Geophys. Res. Lett.*, *21*, 2191–2194, 1994.

Dewey, J. W., Seismic studies with the method of joint hypocenter determination, Ph.D. thesis, Univ. of Calif., Berkeley, 1971.

Dewey, J. W., Relocation of instrumentally recorded pre-1974 earthquakes in the South Carolina region, in *Studies Related to the Charleston, South Carolina, Earthquake of 1886—Tectonics and Seismicity*, *U.S. Geol. Surv. Prof. Pap.*, *1313*, Q1–Q9, 1983.

Dmowska, R., and J. R. Rice, Fracture theory and its seismological applications, in *Continuum Theories in Solid Earth Physics*, vol. III, edited by R. Teisseyre, pp. 187–255, Elsevier Sci., New York, 1985.

Douglas, A., Joint epicentre determination, *Nature*, *215*, 621–623, 1967.

Dziewonski, A. M., and J. H. Woodhouse, Studies of the seismic source using normal-mode theory, *Proc. Int. Sch. Phys. Enrico Fermi*, *LXXXV*, 45–137, 1983.

Dziewonski, A. M., et al., Centroid-moment tensor solutions 1977–1998, *Phys. Earth Planet. Inter.*, 33–115, 1983–1999.

Eaton, J. P., M. E. O'Neill, and J. N. Murdoch, Aftershocks of the 1966 Parkfield-Cholame, California, earthquake: A detailed study, *Bull. Seismol. Soc. Am.*, *60*, 1151–1197, 1970.

Ekstrom, G., and E. R. Engdahl, Earthquake source parameters and stress distribution in the Adak Island region of the central Aleutian Islands, Alaska, *J. Geophys. Res.*, *94*, 15,499–15,519, 1989.

Engdahl, E. R., R. van der Hilst, and R. P. Buland, Global teleseismic earthquake relocation with improved travel times and procedures for depth determination, *Bull. Seismol. Soc. Am.*, *88*, 722–743, 1998.

Gzovsky, M. B., D. N. Osokina, A. A. Lomakin, and B. B. Kudreshova. Stresses, ruptures and earthquake foci (modelling results), in *Regional Study of Seismic Regime* (in Russian), pp. 113–124, Stiinitza, Kishinev, 1974.

Hartzell, S. H., Comparison of seismic waveform inversion results for the rupture history of a finite fault: Application to the 1986 North Palm Springs, California, earthquake, *J. Geophys. Res.*, *94*, 7515–7534, 1989.

Hartzell, S. H., and T. H. Heaton, Inversion of strong ground motion and teleseismic waveform data for the fault rupture history of the 1979 Imperial Valley, California, earthquake, *Bull. Seismol. Soc. Am.*, *73*, 1553–1583, 1983.

Hartzell, S. H., G. S. Stewart, and C. Mendoza, Comparison of $L_1$ and $L_2$ norms in a teleseismic waveform inversion for the slip history of the Loma Prieta, California, earthquake, *Bull. Seismol. Soc. Am.*, *81*, 1518–1539, 1991.

Hauksson, E., State of stress from focal mechanisms before and after the 1992 Landers earthquake sequence, *Bull. Seismol. Soc. Am.*, *84*, 917–934, 1994.

Hauksson, E., Crustal structure and seismicity distributions adjacent to the Pacific and North America plate boundary in southern California, *J. Geophys. Res.*, *105*, 13,875–13,903, 2000.

Henry, C., Teleseismic studies of large submarine earthquakes, Ph.D. thesis, Oxford Univ., Oxford, U. K., 2002.

Henry, C., and S. Das, Aftershock zones of large shallow earthquakes: Fault dimensions, aftershock area expansion, and scaling relations, *Geophys. J. Int.*, *147*, 272–293, 2001.

Henry, C., and S. Das, The $M_w$ 8.2 17 February 1996 Biak, Indonesia, earthquake: Rupture history, aftershocks, and fault plane properties, *J. Geophys. Res.*, *107*(B11), 2312, doi:10.1029/2001JB000796, 2002.

Henry, C., S. Das, and J. H. Woodhouse, The great March 25, 1998 Antarctic plate earthquake: Moment tensor and rupture history, *J. Geophys. Res.*, *105*, 16,097–16,119, 2000.

Husseini, M. I., D. B. Jovanovich, M. J. Randall, and L. B. Freund, The fracture energy of earthquakes, *Geophys. J. R. Astron. Soc.*, *43*, 367–385, 1975.

Hwang, C., E. C. Kao, and B. Parsons, Global derivation of marine gravity anomalies from Seasat, Geosat, ERS-1 and

TOPEX/ POSEIDON altimeter data, *Geophys. J. Int.*, *134*, 449–459, 1998.

Jones, L. E., and S. E. Hough, Analysis of broadband records from the 28 June 1992 Big Bear earthquake: Evidence of a multiple-event source, *Bull. Seismol. Soc. Am.*, *85*, 688–704, 1995.

King, G. C. P., R. S. Stein, and J. Lin, Static stress changes and the triggering of earthquakes, *Bull. Seismol. Soc., Am.*, *84*, 935–953, 1994.

Kisslinger, C., An experiment in earthquake prediction and the May 7, 1986 Andreanof Islands earthquake, *Bull. Seismol. Soc. Am.*, *78*, 218–229, 1988.

Kisslinger, C., and M. Kikuchi, Aftershocks of the Andreanof Islands earthquake of June 10, 1996, and local seismotectonics, *Geophys. Res. Lett.*, *24*, 1883–1886, 1997.

Kostrov, B. V., and S. Das, Idealized models of fault behavior prior to dynamic rupture, *Bull. Seismol. Soc. Am.*, *72*, 679–703, 1982.

Kostrov, B. V., and S. Das, Evaluation of stress and displacement fields due to an elliptical plane shear crack, *Geophys. J. R. Astron. Soc.*, *78*, 19–33, 1984.

Lay, T., and T. C. Wallace, *Modern Global Seismology*, 521 pp., Academic, San Diego, Calif., 1995.

Madariaga, R., On the relation between seismic moment and stress drop in the presence of stress and strength heterogeneity, *J. Geophys. Res.*, *84*, 2243–2249, 1979.

Madariaga, R., S. Peyrat, and K. B. Olsen, Rupture dynamics in 3D: A review, in *Problems in Geophysics for the New Millennium*, pp. 89–110, Ed. Compos., Bologna, Italy, 2000.

Mendoza, C., and S. H. Hartzell, Aftershock patterns and main shock faulting, *Bull. Seismol. Soc. Am.*, *78*, 1438–1449, 1988a.

Mendoza, C., and S. H. Hartzell, Inversion for slip distribution using teleseismic *P* waveforms: North Palm Springs, Borah Peak, and Michoacan earthquakes, *Bull. Seismol. Soc. Am.*, *78*, 1092–1111, 1988b.

Mendoza, C., and S. H. Hartzell, Slip distribution of the 19 September 1985 Michoacan, Mexico, earthquake: Near-source and teleseismic constraints, *Bull. Seismol. Soc. Am.*, *79*, 655–669, 1989.

Mikumo, T., and T. Miyatake, Earthquake sequences on frictional fault model with a non-uniform strength and relaxation times, *Geophys. J. R. Astron. Soc.*, *59*, 497–522, 1979.

Milne, J., and A. W. Lee, *Earthquakes and Other Earth Movements*, 244 pp., K. Paul, Trench, Trubner, London, 1939.

Müller, R. D., W. R. Roest, J. Y. Royer, L. M. Gahagan, and J. G. Sclater, Digital isochrons of the world's ocean floor, *J. Geophys. Res.*, *102*, 3211–3214, 1997.

Olson, A. H., and R. J. Apsel, Finite faults and inverse theory with applications to the 1979 Imperial Valley earthquake, *Bull. Seismol. Soc. Am.*, *72*, 1969–2001, 1982.

Omori, F., On the aftershocks of earthquakes, *Tokyo Imp. Coll. Sci. J.*, *7*, 111–200, 1894.

Oppenheimer, D. H., W. H. Bakun, and A. G. Lindh, Slip partitioning of the Calaveras fault, California, and prospects for future earthquakes, *J. Geophys. Res.*, *95*, 8483–8498, 1990.

Osokina, D. N., and H. U. Tsvetkova, Method of modelling the local stress field near a tectonic fault and at earthquake foci (in Russian), in *Stress and Deformation Fields in the Lithosphere*, pp. 139–162, Nauka, Moscow, 1979.

Pegler, G., Studies in seismotectonics, Ph.D. thesis, Oxford Univ., Oxford, U. K., 1995.

Pegler, G., and S. Das, Analysis of the relationship between seismic moment and fault length for large crustal strike-slip earthquakes between 1977–92, *Geophys. Res. Lett.*, *23*, 905–908, 1996.

Pegler, G., and S. Das, The 1987–92 Gulf of Alaska earthquakes, *Tectonophysics*, *257*, 111–136, 1996.

Perez, O. J., Revised world seismicity catalog (1950–1997) for strong ($M_s \geq 6$) shallow ($h \leq 70$ km) earthquakes, *Bull. Seismol. Soc. Am.*, *89*, 335–341, 1999.

Richter, C. F., Foreshocks and aftershocks, in *Earthquakes in Kern County, California During 1952*, Div. Mines Bull. *171*, 199–202, 1955.

Richter, C. F., *Elementary Seismology*, 768 pp., W. H. Freeman, New York, 1958.

Robinson, D. P., C. Henry, S. Das, and J. H. Woodhouse, Simultaneous rupture along two conjugate planes of the Wharton Basin earthquake, *Science*, *292*, 1145–1148, 2001.

Sandwell, D. T., Marine gravity anomaly from Geosat and ERS 1 satellite altimetry, *J. Geophys. Res.*, *102*, 10,039–10,054, 1997.

Scholz, C., *The Mechanics of Earthquake and Faulting*, 439 pp., Cambridge Univ. Press, New York, 1989.

Smith, S. W., and W. Van de Lindt, Strain adjustments associated with earthquakes associated in southern California, *Bull. Seismol. Soc. Am.*, *59*, 1569–1589, 1969.

Stolte, C., K. C. McNally, R. J. R. Gonzalez, G. W. Simila, A. Reyes, C. Rebollar, L. Munguia, and L. Mendoza, Fine structure of a postfailure Wadati-Benioff zone, *Geophys. Res. Lett.*, *13*, 577–580, 1986.

Tajima, F., and H. Kanamori, Global survey of aftershock area expansion patterns, *Phys. Earth Planet. Int.*, *40*, 77–134, 1985.

Wald, D. J., and T. H. Heaton, Spatial and temporal distribution of slip for the 1992 Landers, California, earthquake, *Bull. Seismol. Soc. Am.*, *84*, 668–691, 1994.

Wald, D. J., T. H. Heaton, and K. W. Hudnut, The slip history of the 1994 Northridge, California, earthquake determined from strong-motion, teleseismic, GPS, and leveling data, *Bull. Seismol. Soc. Am.*, *86*, S49–S70, 1996.

Ward, P. L., J. Gibbs, D. Harlow, and Q. A. Aburto, Aftershocks of the Managua, Nicaragua, earthquake and the tectonic significance of the Tiscapa fault, *Bull. Seismol. Soc. Am.*, *64*, 1017–1029, 1974.

Yamashina, K., Induced earthquakes caused by preceding earthquakes (abstract), *Eos Trans. AGU*, *61*, 292–293, 1980.

Yeats, R. S., K. Sieh, and C. R. Allen, *The Geology of Earthquakes*, 568 pp., Oxford Univ. Press, New York, 1997.

S. Das, Department of Earth Science, University of Oxford, Parks Road, Oxford OX1 3PR, UK. (das@earth.ox.ac.uk)

C. Henry, Oxford Computer Consultants, 2 Cambridge Terrace, Oxford OX1 3PR, UK.

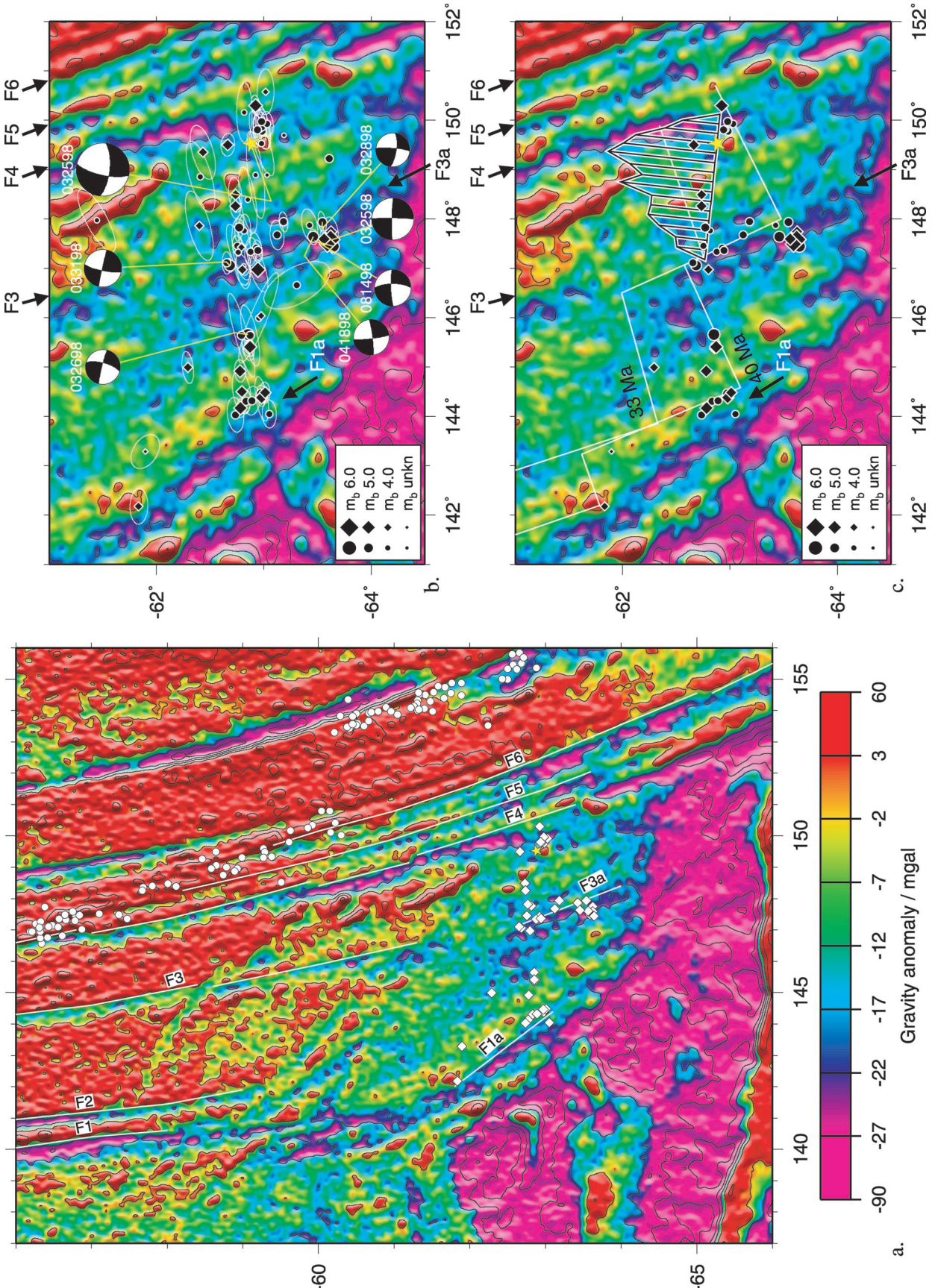
a.
b.
c.
F1
F2
F3
F4
F5
F6
F1a
F3a
-60
-65
140
145
150
155
Gravity anomaly / mgal
60
3
-2
-7
-12
-17
-22
-27
-90
-62°
-64°
142°
144°
146°
148°
150°
152°
032598
033198
032698
041898
081498
032898
032598
$m_b$ 6.0
$m_b$ 5.0
$m_b$ 4.0
$m_b$ unkn
33 Ma
40 Ma

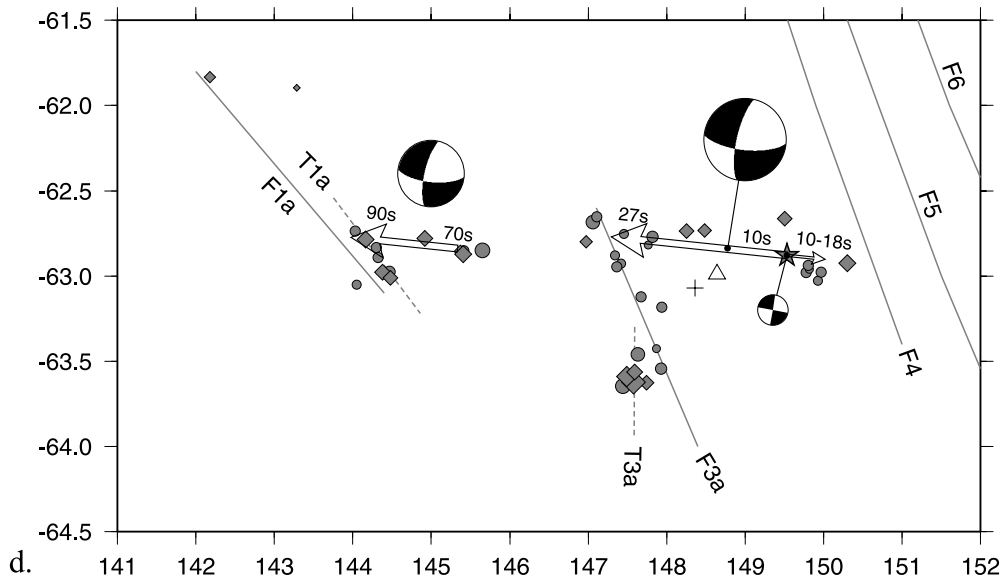


**Figure 6.** (opposite) The 25 March 1998 Antarctic plate earthquake (with a seismic moment of $1.3 \times 10^{21}$ N m). (a) Relocated aftershocks [*Henry et al.*, 2000] for the period 25 March 1998 to 25 March 1999 are shown as diamonds, with the main shock epicenter shown by a star. Only those earthquakes which are located with the semimajor axis of the 90% confidence ellipse <20 km are shown. International Seismological Centre epicenters for the period 1 January 1964 to 31 July 1997 are shown as circles. Marine gravity anomalies from an updated version of *Sandwell and Smith* [1997], illuminated from the east, with contours every 20 mGal, are shown in the background in the epicentral region. Selected linear gravity features are identified by white lines and are labeled F1–F6. F1, F2, and their southward continuation to join F1a compose the George V fracture zone. F4–F6 compose the Tasman fracture zone. (b) An expanded view of the region of the aftershocks. The relocated aftershocks in the first 24 hours are shown as diamonds; the rest are shown as circles. The 90% confidence ellipses are plotted for the locations; earthquakes without confidence ellipses were not successfully relocated and are plotted at the National Earthquake Information Center (NEIC) locations. The yellow star shows the NEIC epicenter for the main shock, with the CMT mechanism of solution 5 from *Henry et al.* [2000]. Available Harvard CMT solutions for the aftershocks are plotted, linked with lines to their centroid locations and then to their relocated epicenters, and are identified by their dates (mmddyy). The location of the linear features identified on Figure 6a are shown by black arrows. (c) Final distribution of moment release for preferred solution 8 of *Henry et al.* [2000]. There are the same gravity anomalies, same linear features, and same epicenters as Figure 6b except that now only earthquakes which are located with the semimajor axis of the 90% confidence ellipse <20 km are shown. Two isochrons from *Müller et al.* [1997] are plotted as white lines. Superimposed graph shows the final moment density, with a peak density of $1.25 \times 10^{19}$ N m km $^{-1}$. Regions of the fault with <15% of this maximum value are excluded in this plot. The baseline of the graph is the physical location of the fault. The spatial and temporal grid sizes used in the inversion for the slip were 5 km × 5 km and 3 s, respectively. (d) Principal features of the main shock rupture process [from *Henry et al.*, 2000]. Arrows show location and directivity for the first and second subevents. Arrows are labeled with start and end times of rupture segments. Focal mechanisms are shown for the initiation, the first subevent plotted at the centroid obtained by *Henry et al.* [2000], and the second subevent. (The second subevent is not well located, and the centroid location is not indicated.) The cross shows the centroid location of moment tensor of the total earthquake obtained by *Henry et al.* [2000], and the triangle shows the Harvard CMT centroid. The same aftershock epicenters as Figure 6c are shown. Linear gravity features are shown as shaded lines, and probable locations of tectonic features T1a and T3a associated with the gravity features F1a and F3a are shown as shaded dashed lines. (See *Henry et al.* [2000] for further details.)

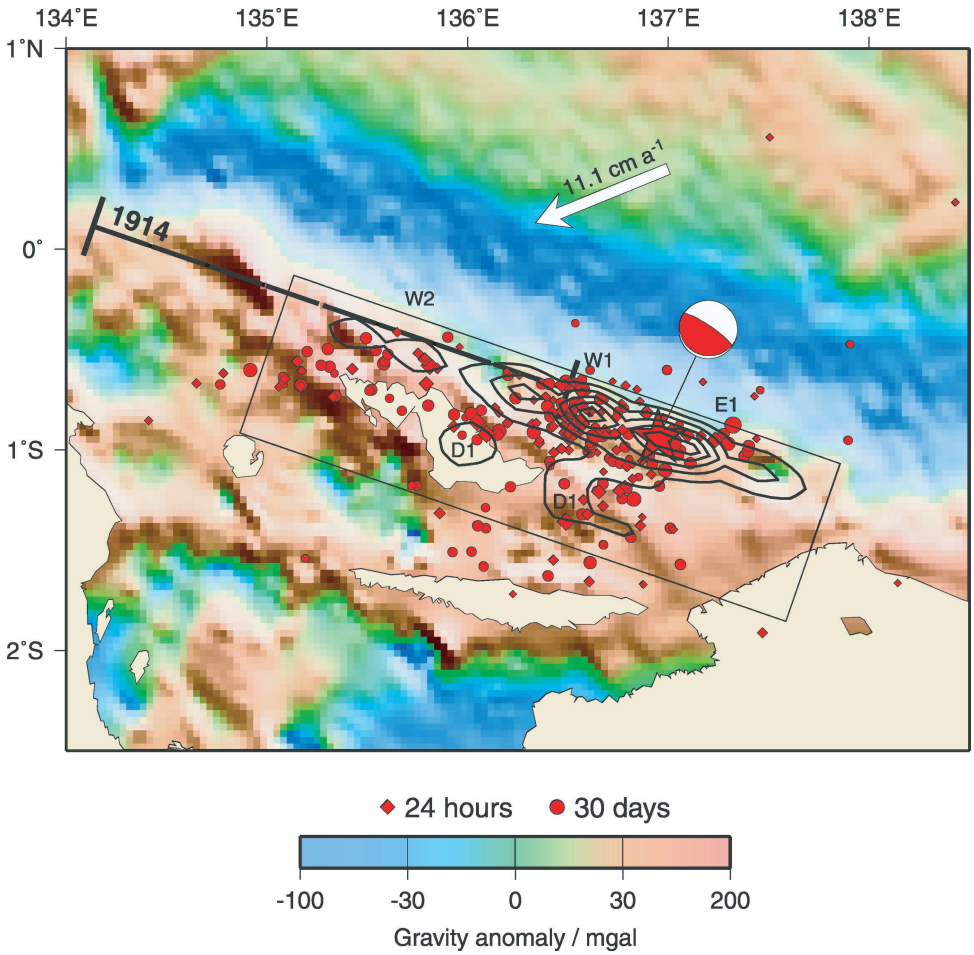


**Figure 11.** Map view of the final moment distribution for the 1996 Biak, Indonesia, earthquake and its aftershocks, together with the CMT solution for the main shock (checked by *Henry and Das* [2002] and found to be the same as the Harvard solution). The main shock epicenter is the red star. The seismic moment was $2.7 \times 10^{21}$ N m. Relocated aftershocks with 90% confidence limits (semimajor axis of error ellipse) <30 km, from 17 February 1996 to 18 March 1996, with size increasing with $m_b$ and symbol (see the key) indicating time of occurrence, are shown. The fault area is indicated by the rectangle. Solid contours at intervals of $10^{20}$ N m km$^{-2}$ show the final moment distribution. The labels W1, W2, E1, and D1 indicate features of the rupture process, with W meaning westward rupture, E meaning eastward rupture, and D meaning downward rupture and 1 and 2 indicating the first and second phases of the rupture propagation in the appropriate direction [*Henry and Das*, 2002]. Marine gravity anomaly, shown in the background, is taken from *Hwang et al.* [1998]. The NUVEL-1A Pacific-Australia plate motion vector is from *DeMets et al.* [1994].